Inhibition of the UFD-1-NPL-4 complex triggers an aberrant immune response in *Caenorhabditis elegans*

Rajneesh Rao[1] , Alejandro Aballay[2], and Jogender Singh[1,*]

[1]Department of Biological Sciences, Indian Institute of Science Education and Research, Mohali, Punjab, 140306, India

[2]Department of Genetics, The University of Texas MD Anderson Cancer Center, Houston, Texas, 77030, USA

[*]For correspondence: jogender@iisermohali.ac.in

Keywords: Colonization, ERAD, GATA transcription factor, immune response, ubiquitin-proteasome system

Abstract

The UFD-1 (ubiquitin fusion degradation 1)-NPL-4 (nuclear protein localization homolog 4) heterodimer is involved in extracting ubiquitinated proteins from several plasma membrane locations, including the endoplasmic reticulum. This heterodimer complex helps in the degradation of ubiquitinated proteins via the proteasome with the help of the AAA+ ATPase CDC-48. While the ubiquitin-proteasome system is known to have important roles in maintaining innate immune responses, the role of the UFD-1-NPL-4 complex in regulating immunity remains elusive. In this study, we investigate the role of the UFD-1-NPL-4 complex in maintaining *Caenorhabditis elegans* innate immune responses. Inhibition of the UFD-1-NPL-4 complex activates an aberrant immune response that reduces the survival of the wild-type worms on the pathogenic bacterium *Pseudomonas aeruginosa* despite diminishing colonization of the gut with the bacterium. This aberrant immune response improves the survival of severely immunocompromised worms on pathogenic bacteria but is detrimental on nonpathogenic bacteria. Transcriptomics studies reveal that the GATA transcription factor ELT-2 mediates the aberrant immune response upon inhibition of the UFD-1-NPL-4 complex. Collectively, our findings show that inhibition of the UFD-1-NPL-4 complex triggers an aberrant immune response that is detrimental to immunocompetent worms under infection conditions but can be advantageous for immunocompromised worms.

Introduction

Maintenance of a healthy proteome involves the degradation of misfolded proteins (Vembar and Brodsky, 2008; Vilchez et al., 2014). Proteasomes are a major site for the degradation of misfolded proteins (Clague and Urbe, 2010; Ding and Yin, 2008). Proteins are tagged for proteasomal degradation by ubiquitin through a series of enzymatic reactions (Dikic, 2017). In addition to the proteasomal degradation of proteins, ubiquitination controls a vast array of cellular signals and functions (Husnjak and Dikic, 2012; Mukhopadhyay and Riezman, 2007). The ubiquitination pathways also have important roles in innate immunity regulation (Garcia-Sanchez et al., 2021; Li et al., 2016). The host ubiquitination pathways are involved in the targeting of bacterial proteins, lipopolysaccharides, and bacteria-containing vacuoles, resulting in selective macroautophagy or xenophagy of bacterial pathogens (Chai et al., 2019; Haldar et al., 2015; Otten et al., 2021; Tripathi-Giesgen et al., 2021). Because of the important roles of ubiquitination in host defenses, bacterial pathogens have evolved multiple strategies to target the host ubiquitination pathways (Bomberger et al., 2011; Herhaus and

Dikic, 2018; Ribet and Cossart, 2018). Therefore, it is possible that inhibition of the ubiquitination pathways would activate immune responses via compensatory mechanisms.

The proteasomal degradation requires ubiquitin-tagged proteins to be unfolded and extracted from macromolecular complexes (Boom and Meyer, 2018). CDC-48 (VCP/p97 in vertebrates) is a highly conserved AAA+ ATPase that uses its protein unfoldase activity to extract a variety of ubiquitinated polypeptides from membranes or macromolecular complexes (Bodnar and Rapoport, 2017; Meyer et al., 2012). CDC-48 uses different cofactor proteins to recognize its client proteins (Meyer et al., 2012). The UFD-1 (ubiquitin fusion degradation 1)-NPL-4 (nuclear protein localization homolog 4) heterodimer is a CDC-48 cofactor that is involved in the extraction of misfolded and ubiquitinated proteins from several plasma membrane locations, including the endoplasmic reticulum (ER) (Meyer et al., 2000; Wolf and Stolz, 2012; Ye et al., 2001). Therefore, the UFD-1-NPL-4 complex is critical for the ER-associated degradation (ERAD) of misfolded proteins (Wu and Rapoport, 2018). In addition to ERAD, the ER has evolved other strategies to deal with misfolded proteins (Singh, 2023), including a series of unfolded protein response (UPR) pathways that enhance the folding capacity of the ER by synthesis of molecular chaperones and reduction of protein translation (Hetz et al., 2015). The ER-UPR pathways are required for an optimum immune response (Engel and Barton, 2010; Richardson et al., 2010; Sun et al., 2012). However, the role of the UFD-1-NPL-4 complex, which is required for ERAD, in regulating immune responses remains poorly explored. Because ubiquitin-dependent pathways have important roles in immunity, it will be interesting to explore the role of the UFD-1-NPL-4 complex in regulating immune responses.

In this study, we showed that the inhibition of the UFD-1-NPL-4 complex results in the activation of an aberrant immune response in *Caenorhabditis elegans*. The wild-type worms had a significant reduction in survival on the pathogenic bacterium *Pseudomonas aeruginosa* despite having diminished colonization of the gut with the bacterium. Inhibition of the UFD-1-NPL-4 complex also led to diminished bacterial colonization in mutants of ER-UPR and immunity pathways. The diminished bacterial colonization improved the survival of severely immunocompromised mutants on pathogenic bacteria. However, on nonpathogenic bacteria, on which the severely immunocompromised mutants exhibit a normal lifespan, inhibition of the UFD-1-NPL-4 complex resulted in a significant reduction in lifespan. Transcriptomic studies revealed that inhibition of the UFD-1-NPL-4 complex resulted in the activation of the intracellular pathogen response. Analysis for transcription factor enrichment for upregulated genes identified that the GATA transcription factor ELT-2 mediated the

aberrant immune response upon inhibition of the UFD-1-NPL-4 complex. Thus, our studies demonstrated that inhibition of the UFD-1-NPL-4 complex triggers an aberrant immune response that is detrimental to immunocompetent worms under infection conditions but can be advantageous for immunocompromised worms.

Results

Inhibition of the UFD-1-NPL-4 complex reduces survival of *C. elegans* on *P. aeruginosa*

To explore the role of the UFD-1-NPL-4 complex in the innate immune response of *C. elegans*, we knocked down *ufd-1* and *npl-4* by RNA interference (RNAi) and studied the survival of the worms on the pathogenic bacterium *P. aeruginosa* PA14. Knockdown of *ufd-1* and *npl-4* resulted in a significant reduction in the survival of N2 wild-type worms on *P. aeruginosa* compared to worms grown on control RNAi (Figure 1A). The animals also had a reduced lifespan on *Escherichia coli* HT115 upon knockdown of *ufd-1* and *npl-4* (Figure 1B). The relationship between *C. elegans* innate immunity and longevity pathways is complex. Mutants that have reduced lifespan but improved immunity have been identified (Amrit et al., 2019; Otarigho and Aballay, 2021; Ren and Ambros, 2015). Moreover, immunocompromised animals such as mutants of the MAP kinase pathway mediated by NSY-1/SEK-1/PMK-1 have a normal lifespan despite having significantly reduced survival on pathogenic bacteria (Kim et al., 2002; Liberati et al., 2004). Therefore, we explored the mechanisms that led to the reduced survival of *ufd-1* and *npl-4* knockdown animals on *P. aeruginosa*. Colonization of the gut with *P. aeruginosa* is a major determinant of infection and survival of *C. elegans* under slow-killing conditions (Das et al., 2023; Tan et al., 1999). Because knockdown of *ufd-1* and *npl-4* reduced survival on *P. aeruginosa*, we asked whether the animals had enhanced colonization of the gut with *P. aeruginosa* after *ufd-1* and *npl-4* RNAi. Surprisingly, we observed that *ufd-1* and *npl-4* knockdown resulted in reduced colonization of the gut with *P. aeruginosa* (Figure 1C and 1D). To validate further, we performed the colony-forming unit assay (CFU) upon knockdown of *ufd-1* and *npl-4*. There was a significant decline in the CFU per worm in *ufd-1* and *npl-4* knockdown worms, indicating reduced numbers of live bacteria in these worms (Figure 1E).

To confirm the specificity of the RNAi knockdowns and rule out potential off-target effects, we examined transcript levels of *ufd-1* and *npl-4* following RNAi treatment. RNAi against *ufd-1* significantly reduced *ufd-1* mRNA levels without reducing *npl-4* expression, while *npl-4* RNAi specifically downregulated *npl-4* transcripts with no impact on *ufd-1* mRNA levels (Figure 1—figure supplement 1A and B). Additionally, alignment of *ufd-1* and

npl-4 mRNA sequences against the *C. elegans* transcriptome revealed no significant similarity to other genes, supporting the specificity of the RNAi constructs. Moreover, the *ufd-1* and *npl-4* RNA sequences do not share significant sequence similarity. Therefore, the highly similar phenotypes observed in *ufd-1* and *npl-4* knockdown animals, including shortened lifespan, reduced survival on *P. aeruginosa*, and decreased intestinal colonization with *P. aeruginosa*, strongly suggest that these outcomes result from the disruption of the functional UFD-1-NPL-4 complex.

Reduced colonization of the gut by *P. aeruginosa* could be because of reduced uptake of the bacterium in *ufd-1* and *npl-4* knockdown animals. The rate of pharyngeal pumping is an indicator of the uptake of bacterial food. We studied whether inhibition of *ufd-1* and *npl-4* affected the pharyngeal pumping rate. The knockdown of *ufd-1* and *npl-4* did not affect the pharyngeal pumping rate (Figure 1—figure supplement 2A), indicating that the reduced colonization was unlikely due to the reduced uptake of bacteria. Next, we tested whether exposure to *P. aeruginosa* affected the pharyngeal pumping in *ufd-1* and *npl-4* knockdown animals. Exposure to *P. aeruginosa* for 12 hours resulted in a minimal reduction in the pharyngeal pumping rate in *ufd-1* and *npl-4* knockdown animals compared to control animals (Figure 1—figure supplement 2B). These results suggested that the reduced colonization of *ufd-1* and *npl-4* knockdown animals by *P. aeruginosa* was unlikely because of the reduced uptake of bacteria.

The clearance of intestinal contents through the defecation motor program (DMP) is known to influence gut colonization by *P. aeruginosa* in *C. elegans* (Das et al., 2023). It is therefore conceivable that knockdown of the UFD-1-NPL-4 complex might increase defecation frequency, thereby promoting the physical expulsion of bacteria and resulting in reduced gut colonization. To test this possibility, we measured DMP rates in animals subjected to *ufd-1* and *npl-4* RNAi. Contrary to this hypothesis, both *ufd-1* and *npl-4* knockdown animals exhibited a significant reduction in defecation frequency compared to control RNAi-treated animals (Figure 1—figure supplement 2C). This reduction in DMP rate persisted even after 12 hours of exposure to *P. aeruginosa* (Figure 1—figure supplement 2D). Thus, the change in the DMP rate in *ufd-1* and *npl-4* knockdown animals is unlikely to be the reason for the reduced gut colonization by *P. aeruginosa*.

Taken together, these results suggested that the inhibition of the UFD-1-NPL-4 complex reduced the survival of *C. elegans* on *P. aeruginosa* despite diminished colonization of the gut with the bacterium. Because *ufd-1* and *npl-4* RNAi led to very similar phenotypes,

we further used only *ufd-1* RNAi to decipher the mechanisms of reduced survival and diminished colonization on *P. aeruginosa*.

Reduced colonization with *P. aeruginosa* upon *ufd-1* knockdown is independent of the ER-UPR pathways

Knockdown of the UFD-1-NPL-4 complex is known to cause ER stress, resulting in the upregulation of the ER-UPR pathways (Mouysset et al., 2006; Sasagawa et al., 2007). Because ER stress and UPR pathways modulate innate immunity (Richardson et al., 2010; Singh and Aballay, 2017; Sun et al., 2012), we asked whether the ER-UPR pathways were involved in the regulation of survival and colonization of *ufd-1* knockdown animals on *P. aeruginosa*. We studied the survival and colonization of mutants of different ER-UPR pathways, including *xbp-1(tm2482)*, *atf-6(ok551)*, and *pek-1(ok275)* on *P. aeruginosa*. The survival of *xbp-1(tm2482)* animals upon *ufd-1* knockdown was indistinguishable from that of the control animals (Figure 2A). However, *ufd-1* knockdown resulted in significantly reduced gut colonization with *P. aeruginosa* in *xbp-1(tm2482)* animals (Figure 2B and 2C).

To further examine the role of XBP-1 in this context, we assessed the effect of *ufd-1* knockdown in animals neuronally overexpressing the constitutively active spliced form of XBP-1 (XBP-1s), which has been previously associated with enhanced longevity (Taylor and Dillin, 2013). Knockdown of *ufd-1* resulted in the reduced survival of XBP-1s-overexpressing animals on *P. aeruginosa*, despite a concurrent decrease in bacterial colonization of the gut (Figure 2—figure supplement 1A-C). This indicated that the XBP-1 pathway was not required for the reduced *P. aeruginosa* colonization of *ufd-1* knockdown animals.

The *atf-6(ok551)* animals exhibited reduced survival on *P. aeruginosa* upon *ufd-1* RNAi compared to the control RNAi (Figure 2D). Similar to N2, *ufd-1* knockdown resulted in reduced colonization of the gut with *P. aeruginosa* in *atf-6(ok551)* animals (Figure 2E and 2F). The *pek-1(ok275)* animals exhibited similar phenotypes of reduced survival and diminished colonization on *P. aeruginosa* upon *ufd-1* knockdown (Figure 2G-I). These results indicated that the reduced colonization and survival of *ufd-1* knockdown animals on *P. aeruginosa* were independent of the ER-UPR pathways.

Reduced colonization with *P. aeruginosa* upon *ufd-1* knockdown is independent of the major immunity pathways

Next, we tested whether any of the immunity pathways were involved in regulating the reduced colonization by *ufd-1* knockdown. To this end, we studied the survival and colonization of mutants of different immunity pathways on *P. aeruginosa* upon knockdown of *ufd-1*. The *pmk-1(km25)* animals, which are part of a MAP kinase pathway mediated by NSY-1/SEK-1/PMK-1 (Kim et al., 2002), had a similar survival rate on control and *ufd-1* RNAi (Figure 3A). However, *ufd-1* knockdown significantly reduced colonization in *pmk-1(km25)* animals (Figure 3B and 3C). This indicated that the *pmk-1* pathway is unlikely to be involved in mediating *ufd-1* knockdown effects, and the similar survival rate of control and *ufd-1* RNAi animals is merely coincidental. Indeed, a mutant of the upstream regulator of the PMK-1 pathway, the Toll/interleukin-1 receptor domain protein (TIR-1) (Liberati et al., 2004; Peterson et al., 2022), exhibited phenotypes similar to *pmk-1(km25)* animals ((Figure 3—figure supplement 1A-C).

The mutants of the TGF-β/DBL-1 (Mallo et al., 2002) and TFEB/HLH-30 (Visvikis et al., 2014) immunity pathways also exhibited phenotypes similar to *pmk-1(km25)* animals. The knockdown of *ufd-1* resulted in significantly reduced colonization of *dbl-1(nk3)* and *hlh-30(tm1978)* animals without affecting their survival on *P. aeruginosa* (Figure 3D-I). These results indicated that the reduced colonization with *P. aeruginosa* upon *ufd-1* knockdown was independent of these immunity pathways.

Inhibition of the UFD-1-NPL-4 complex improves survival of severely immunocompromised *C. elegans* on *P. aeruginosa*

Knockdown of *ufd-1* reduced colonization in wild-type animals as well as mutants of ER-UPR and innate immunity pathways. Interestingly, despite variable survival rates on control RNAi, all strains had similar survival rates upon knockdown of *ufd-1* (Figure 4—figure supplement 1). We reasoned that *ufd-1* knockdown might lead to an aberrant immune response that results in diminished gut colonization by *P. aeruginosa* and reduces the survival of healthy but not immunocompromised animals. If this were the case, knockdown of the UFD-1-NPL-4 complex might improve the survival of severely immunocompromised animals by activating a compensatory immune response. In *C. elegans*, the canonical p38 MAP kinase signaling cascade consists of NSY-1 (ASK1 MAPKKK), SEK-1 (MKK3/MKK6 MAPKK), and PMK-1 (p38 MAPK) (Kim et al., 2002). Compared to *pmk-1* knockout, the knockout of *sek-1* leads to more severe effects on survival upon infection with *P. aeruginosa* (Meng et al., 2021). Indeed, we observed that most of the *sek-1(km4)* animals on control RNAi died within 24 hours of exposure to *P. aeruginosa* (Figure 4A). Importantly, the

knockdown of *ufd-1* resulted in a significant improvement in the survival of *sek-1(km4)* animals (Figure 4A). To test whether the improved survival of *sek-1(km4)* animals upon the knockdown of *ufd-1* was because of inhibition of the UFD-1-NPL-4 complex, we studied the survival of *sek-1(km4)* animals upon *npl-4* RNAi. The knockdown of *npl-4* also resulted in significantly enhanced survival of *sek-1(km4)* animals (Figure 4A).

Knockdown of both *ufd-1* and *npl-4* in *sek-1(km4)* animals resulted in reduced gut colonization by *P. aeruginosa* compared to control RNAi (Figure 4B and 4C). Because *sek-1(km4)* animals do not have a reduced lifespan on *E. coli* diet (Kim et al., 2002), we studied how inhibition of the UFD-1-NPL-4 complex affected the lifespan of *sek-1(km4)* animals. We reasoned that if the inhibition of the UFD-1-NPL-4 complex resulted in a heightened aberrant immune response, it should result in a reduced lifespan of *sek-1(km4)* animals on *E. coli* despite improving their survival on *P. aeruginosa*. Indeed, the knockdown of *ufd-1* and *npl-4* significantly reduced the lifespan of *sek-1(km4)* animals on *E. coli* HT115 (Figure 4D). These results suggested that inhibition of the UFD-1-NPL-4 complex led to an aberrant immune response, which improves survival of severely immunocompromised animals under infection conditions but reduces survival of such animals under non-infection conditions.

To further establish that inhibition of the UFD-1-NPL-4 complex resulted in the improved survival of severely immunocompromised animals on *P. aeruginosa*, we created a *dbl-1(nk3);pmk-1(km25)* double mutant. The TGF-β/DBL-1 and p38 MAPK/PMK-1 control immunity via parallel pathways (Singh and Aballay, 2020), and the *dbl-1(nk3);pmk-1(km25)* animals show reduced survival on *P. aeruginosa* compared to individual mutants (Figure 4E). The knockdown of *ufd-1* resulted in improved survival (Figure 4E) and reduced colonization (Figure 4F and 4G) of *dbl-1(nk3);pmk-1(km25)* animals on *P. aeruginosa*. Taken together, these data showed that inhibition of the UFD-1-NPL-4 complex improved the survival of severely immunocompromised animals on *P. aeruginosa*.

Knockdown of *ufd-1* results in the upregulation of protease and intracellular pathogen response genes

To understand the molecular basis of the phenotypes observed upon knockdown of *ufd-1*, we used RNA sequencing to focus on transcriptional changes induced by *ufd-1* RNAi. Of the 439 differentially regulated genes, 319 were upregulated, while 120 were downregulated (Figure 5A and Table S1). Gene ontology (GO) analysis for biological processes for upregulated genes showed enrichment for innate immune response (Figure 5B). As *ufd-1* is required for ERAD, different ER-UPR pathway genes were also enriched in the upregulated genes. In

addition, enrichment for proteolysis genes was also observed. GO analysis for cellular components and molecular function for upregulated genes showed enrichment for lysosomes and peptidase activities, respectively (Figure 5C and 5D). These results indicated that the knockdown of *ufd-1* might result in increased proteolysis activities via lysosomes. GO analysis for biological processes for downregulated genes also showed enrichment for innate immune response (Figure 5—figure supplement 1). This indicated that *ufd-1* might be required for the expression of some innate immune response genes. GO analysis for cellular components and molecular function for downregulated genes primarily identified functions related to nucleosomes (Figure 5—figure supplement 1B and 1C). Indeed, UFD-1 is known to localize to the nucleus and is required for chromatin stability (Mouysset et al., 2008).

Next, we compared the upregulated genes with previously published gene expression data using WormExp (Yang et al., 2016b). Interestingly, we observed that the *ufd-1* RNAi upregulated genes had a very high overlap with genes upregulated by intracellular pathogens *Nematocida parisii* (Bakowski et al., 2014) (Figure 5E) and Orsay virus (Sarkies et al., 2013) (Figure 5F). Infection with the intracellular pathogens *N. parisii* and Orsay virus results in the activation of an intracellular pathogen response (IPR), which includes several *p*rotein containing *ALS*2CR12 signature (*pals*) genes as well as genes involved in proteolysis (Bakowski et al., 2014; Sarkies et al., 2013). Indeed, *ufd-1* RNAi resulted in the upregulation of several *pals* and proteolysis genes (Table S1). These results indicated that the knockdown of *ufd-1* might mimic an intracellular pathogen infection and result in the activation of the IPR.

GATA transcription factor ELT-2 mediates the *ufd-1* knockdown phenotypes

To identify the genes downstream of *ufd-1* knockdown that were responsible for reduced colonization, we knocked down individual genes that were upregulated upon *ufd-1* RNAi and studied colonization of the gut with *P. aeruginosa*. We hypothesized that the reduced colonization might be because of increased expression of proteolysis genes. Therefore, we knocked down the proteolysis genes that were upregulated by *ufd-1* RNAi. Knockdown of the protease genes *cpr-1*, *asp-12*, and Y71H2AR.25 led to a significant increase in colonization in *ufd-1* knockdown animals (Figure 6—figure supplement 1A), suggesting that increased expression of protease genes might be responsible for reduced colonization. Because *ufd-1* knockdown also resulted in the upregulation of several *pals* genes, which are part of the IPR, we next targeted the *pals* genes upregulated by *ufd-1* RNAi. Knockdown of the *pals* genes, *pals-9*, *pals-14*, *pals-16*, *pals-17*, and *pals-29*, resulted in a significant increase in

colonization in *ufd-1* knockdown animals (Figure 6—figure supplement 1B). These results indicated that some of the proteases and IPR genes are involved in the regulation of colonization in *ufd-1* knockdown animals. It is also likely that these genes function redundantly, and multiple genes contribute to the observed phenotype.

To identify the transcription factors that regulate the diminished colonization and reduced survival phenotype of *ufd-1* knockdown, we carried out transcription factor enrichment analysis for upregulated genes using WormExp. The *ufd-1* RNAi upregulated genes substantially overlapped with the genes regulated by the GATA transcription factor ELT-2 (Dineen et al., 2018; Mann et al., 2016) (Figure 6A and 6B). Indeed, ELT-2 is known to regulate the expression of protease and *pals* genes (Mann et al., 2016). To assess whether ELT-2 contributes to the phenotypes associated with *ufd-1* knockdown, we conducted double RNAi experiments in N2 animals targeting both *ufd-1* and *elt-2* and examined *P. aeruginosa* colonization. The double knockdown of *ufd-1* and *elt-2* did not compromise RNAi efficiency, as evidenced by significantly reduced *ufd-1* mRNA levels and diminished ELT-2::GFP signal (Figure 6—figure supplement 2A and B). Importantly, knockdown of *elt-2* resulted in a significant increase in *P. aeruginosa* colonization in *ufd-1* knockdown animals (Figure 6C and 6D). Similar to N2 worms, the knockdown of *elt-2* resulted in a significant increase in *P. aeruginosa* colonization in *ufd-1* knockdown *sek-1(km4)* animals (Figure 6E and 6F). Because *ufd-1* knockdown in *sek-1(km4)* worms improves their survival on *P. aeruginosa* (Figure 4A), we also studied whether *elt-2* was responsible for the increased survival of *sek-1(km4)* worms upon *ufd-1* knockdown. Indeed, the knockdown of *elt-2* abolished the beneficial effects of *ufd-1* knockdown on the survival of *sek-1(km4)* worms on *P. aeruginosa* (Figure 6G).

To determine whether ELT-2 activation alone is sufficient to recapitulate the phenotypes observed upon UFD-1-NPL-4 complex inhibition, we analyzed animals overexpressing ELT-2. Similar to *ufd-1* knockdown, ELT-2 overexpression led to a significant reduction in the colonization of the gut by *P. aeruginosa* (Figure 6—figure supplement 3A and 3B). However, overexpression of ELT-2 did not alter the survival of worms on *P. aeruginosa* (Figure 6—figure supplement 3C). Taken together, these findings suggest that the phenotypes triggered by disruption of the UFD-1-NPL-4 complex are partially mediated by ELT-2. However, additional pathways, yet to be identified, likely cooperate with ELT-2 to regulate both pathogen resistance and host survival.

Discussion

In this study, we show that inhibition of the UFD-1-NPL-4 complex leads to an aberrant immune response in *C. elegans*. Suppression of this complex leads to reduced gut colonization with *P. aeruginosa* in wild-type animals as well as mutants of different ER-UPR and immunity pathways. Despite the reduction in pathogen load, the wild-type animals exhibit reduced survival, indicative of a detrimental immune response. However, immunocompromised mutants, which have significantly reduced survival on pathogenic bacteria, exhibit reduced colonization and improved survival on inhibition of the UFD-1-NPL-4 complex. This indicates that the immune response activated by the inhibition of the UFD-1-NPL-4 complex compensates for the dampened immune response of the immunocompromised mutants. Despite beneficial effects on the survival on pathogenic bacteria, inhibition of the UFD-1-NPL-4 complex leads to adverse effects on the lifespan of immunocompromised mutants. This is because the immunocompromised mutants have a normal lifespan on nonpathogenic bacteria, and the aberrant immune response becomes detrimental on such bacterial diets.

Previous studies have shown that hyperactivation of immune pathways can negatively affect organismal development. For example, sustained activation of the p38 MAPK pathway impairs development in *C. elegans* (Cheesman et al., 2016; Kim et al., 2016), and excessive activation of the IPR also leads to developmental defects (Lažetić et al., 2023). Similar to our current study, recent work has demonstrated that heightened immune responses can reduce gut pathogen load while paradoxically decreasing host survival during infection (Ghosh and Singh, 2024; Peterson et al., 2022). However, our study uniquely shows that while such heightened immune responses are detrimental to immunocompetent animals, they can be beneficial in the context of immunodeficiency.

We find that the knockdown of *ufd-1* led to the upregulation of several genes that are part of the IPR activated by intracellular pathogens *N. parisii* and Orsay virus (Bakowski et al., 2014; Sarkies et al., 2013). The ubiquitination components have been shown to be required for targeting the intracellular pathogen *N. parisii* (Bakowski et al., 2014). As a counterattack, the pathogen probably targets the ubiquitin-proteasome system of the host (Bakowski et al., 2014). Therefore, the intracellular pathogens *N. parisii* and Orsay virus might activate the IPR by inhibiting the ubiquitin-proteasome system (Bakowski et al., 2014; Reddy et al., 2019). We show that inhibition of the UFD-1-NPL-4 complex activates the IPR. The activation of the IPR by the inhibition of the UFD-1-NPL-4 complex could be a consequence of the direct inhibition of this complex itself or an indirect perturbation of the

proteasomal degradation of proteins. In future studies, it will be intriguing to decipher whether intracellular pathogens target the UFD-1-NPL-4 complex.

We demonstrate that the GATA transcription factor ELT-2 mediated the aberrant response downstream of the inhibition of the UFD-1-NPL-4 complex. ELT-2 is known to be required for defense as well as recovery responses against a variety of pathogens (Head and Aballay, 2014; Shapira et al., 2006; Yang et al., 2016a). Previous studies have reported interactions of ELT-2 with the proteasome system. The non-proteolytic activity of the 19S proteasome subunit RPT-6 was shown to regulate the ELT-2-mediated immune response (Olaitan and Aballay, 2018). Another study showed that the bacterial pathogen *Burkholderia pseudomallei* leads to the downregulation of ELT-2 target genes (Lee et al., 2013). It was demonstrated that the downregulation of ELT-2 targets was associated with the degradation of ELT-2 protein by the host ubiquitin-proteasome system. Therefore, multiple mechanisms could regulate the activity of ELT-2 via the ubiquitin-proteasome system. In future studies, it will be interesting to study how inhibition of the UFD-1-NPL-4 complex modulates the activities of the GATA transcription factor ELT-2.

Materials and Methods

Key Resources Table				
Reagent type (species) or resource	**Designation**	**Source or reference**	**Identifiers**	**Additional information**
strain, strain background (*Escherichia coli*)	OP50	*Caenorhabditis* Genetics Center (CGC)	OP50	
strain, strain background (*E. coli*)	HT115(DE3)	Source BioScience	HT115(DE3)	
strain, strain background (*Pseudomonas aeruginosa*)	PA14	Frederick M Ausubel laboratory	PA14	
strain, strain background (*P. aeruginosa*)	PA14-GFP	Frederick M Ausubel laboratory	PA14-GFP	

strain, strain background (*Caenorhabditis elegans*)	N2 Bristol	CGC	N2	
strain, strain background (*C. elegans*)	*sek-1(km4)*	CGC	KU4	
strain, strain background (*C. elegans*)	*pmk-1(km25)*	CGC	KU25	
strain, strain background (*C. elegans*)	*dbl-1(nk3)*	CGC	NU3	
strain, strain background (*C. elegans*)	*hlh-30(tm1978)*	CGC	JIN1375	
strain, strain background (*C. elegans*)	*xbp-1(tm2482)*	NBRP, Japan	*xbp-1(tm2482)*	
strain, strain background (*C. elegans*)	*pek-1(ok275)*	CGC	RB545	
strain, strain background (*C. elegans*)	*atf-6(ok551)*	CGC	RB772	
strain, strain background (*C. elegans*)	*tir-1(qd4)*	CGC	RB1085	
strain, strain background (*C. elegans*)	*uthIs270 [rab-3p::xbp-1s (constitutively active) + myo-2p::tdTomato]*	CGC	AGD927	
strain, strain background (*C. elegans*)	*glo-4(ok623); gaIs290 [elt-2::TY1::EGFP::3xFLAG(92C12) + unc-119(+)]*	CGC	SD1949	
strain, strain background (*C. elegans*)	*dbl-1(nk3);pmk-1(km25)*	This study	*dbl-1(nk3);pmk-1(km25)*	Materials and methods section

strain, strain background (*C. elegans*)	*jsnEx3 [elt-2p::elt-2 + myo-2p::mCherry]*	This study	*elt-2*_OE	Materials and methods section
sequence-based reagent	Pan-act_qPCR_F	This study	qPCR primers	TCGGTATGGGACAGAAGGAC
sequence-based reagent	Pan-act_qPCR_R	This study	qPCR primers	CATCCCAGTTGGTGACGATA
sequence-based reagent	npl-4_qPCR_F	This study	qPCR primers	AATGGAGGAAGCGGCAATGA
sequence-based reagent	npl-4_qPCR_R	This study	qPCR primers	TCCACAGTTCCACACAGCTC
sequence-based reagent	ufd-1_qPCR_F	This study	qPCR primers	GGTCGTGTTTCATTCCTTCG
sequence-based reagent	ufd-1_qPCR_R	This study	qPCR primers	TTGCCTCCACGGAAGACATT
sequence-based reagent	npl-4_RNAi_F	This study	Cloning primers	GCTCCCGGGATGGTACTTGAAGTCCCTCA
sequence-based reagent	npl-4_RNAi_R	This study	Cloning primers	AGGTCTAGAATCGGCAGCTGGCAATCCAC
sequence-based reagent	elt-2_OE_F	This study	Cloning primers	CGTCTGCAGCTGATTGTTTCAGAACACCC
sequence-based reagent	elt-2_OE_R	This study	Cloning primers	CGACCCGGGAAGTAGGGTACACATGTTTG
software, algorithm	GraphPad Prism 8	GraphPad Software	RRID:SCR_002798	https://www.graphpad.com/scientificsoftware/prism/
software, algorithm	Photoshop CS5	Adobe	RRID:SCR_014199	https://www.adobe.com/products/photoshop.html

software, algorithm	ImageJ	NIH	RRID:SCR_003070	https://imagej.nih.gov/ij/

Bacterial strains

The following bacterial strains were used in the current study: *Escherichia coli* OP50, *E. coli* HT115(DE3), *Pseudomonas aeruginosa* PA14, and *P. aeruginosa* PA14 expressing green fluorescent protein (*P. aeruginosa* PA14-GFP). The cultures of *E. coli* OP50, *E. coli* HT115(DE3), and *P. aeruginosa* PA14 were grown in Luria-Bertani (LB) broth at 37°C. The *P. aeruginosa* PA14-GFP cultures were grown in LB broth with 50 µg/mL kanamycin at 37°C.

***C. elegans* strains and growth conditions**

C. elegans hermaphrodites were maintained at 20°C on nematode growth medium (NGM) plates seeded with *E. coli* OP50 as the food source unless otherwise indicated. Bristol N2 was used as the wild-type control unless otherwise indicated. The following strains were used in the study: KU4 *sek-1(km4),* KU25 *pmk-1(km25),* NU3 *dbl-1(nk3),* JIN1375 *hlh-30(tm1978), xbp-1(tm2482),* RB545 *pek-1(ok275),* RB772 *atf-6(ok551),* and RB1085 *tir-1(qd4)*, AGD927 *uthIs270 [rab-3p::xbp-1s (constitutively active) + myo-2p::tdTomato]*, and SD1949 *glo-4(ok623);gaIs290 [elt-2::TY1::EGFP::3xFLAG(92C12) + unc-119(+)]*. Some of the strains were obtained from the Caenorhabditis Genetics Center (University of Minnesota, Minneapolis, MN). The *dbl-1(nk3);pmk-1(km25)* strain was obtained by a standard genetic cross.

Construction of the *npl-4* RNAi clone

The 1581-base-pair full-length cDNA of *npl-4.1* was amplified using the forward primer 5'-GCTCCCGGGATGGTACTTGAAGTCCCTCA -3' and the reverse primer 5'-AGGTCTAGAATCGGCAGCTGGCAATCCAC -3'. Because the nucleotide sequence of the *npl-4.1* gene is 99% identical to that of the *npl-4.2* gene, the cloned cDNA will target both of these genes. Therefore, the clone is referred to as *npl-4*. The fragment was cloned into the SmaI and XbaI sites of pL4440 (Open Biosystems) and transformed into *E. coli* HT115(DE3) cells.

Plasmid constructs and generation of transgenic *C. elegans*

For overexpression of *elt-2*, the *elt-2* gene along with its promoter region (1980-bp upstream) was amplified from genomic DNA of N2 animals. The gene, including its stop codon, was cloned in the pPD95.77 plasmid using the restriction sites PstI and SmaI. N2 worms were microinjected with *elt-2p::elt-2* plasmid along with pCFJ90 (*myo-2p::mCherry*) as a coinjection marker to generate the overexpression strain, *jsnEx3 [elt-2p::elt-2 + myo-2p::mCherry]*. The *elt-2p::elt-2* plasmid was used at a concentration of 50 ng/µl, while the coinjection marker was used at a concentration of 5 ng/µl.

RNA interference (RNAi)

RNAi was used to generate loss-of-function phenotypes by feeding worms with *E. coli* strain HT115(DE3) expressing double-stranded RNA homologous to a target *C. elegans* gene. RNAi was carried out as described previously (Das et al., 2023). Briefly, *E. coli* HT115(DE3) with the appropriate vectors were grown in LB broth containing ampicillin (100 µg/mL) at 37°C overnight on a shaker, concentrated ten times, and plated onto RNAi NGM plates containing 100 µg/mL ampicillin and 3 mM isopropyl β-D-thiogalactoside (IPTG). The plated bacteria were allowed to grow overnight at 37°C. For synchronization of worms, gravid adults were transferred to RNAi-expressing bacterial lawns and allowed to lay eggs for 2 hours. The gravid adults were removed, and the eggs were incubated at 20°C for 96 hours. For protease and IPR genes' co-RNAi with *ufd-1*, *E. coli* HT115(DE3) with the appropriate vectors were grown separately at 37°C overnight until growth saturation. Then, the RNAi cultures were mixed in a ratio of 1:1, concentrated ten times, and plated onto RNAi plates, followed by overnight growth at 37°C. We used all the protease and *pals* genes that were upregulated upon *ufd-1* RNAi and were present in the Ahringer RNAi library. For experiments involving *elt-2* RNAi, the worms were grown on the control *gfp* RNAi (GFP) and *ufd-1* RNAi for 48 hours at 20°C to obtain the L4 stage worms. Afterward, the worms grown on *gfp* RNAi were transferred to GFP+*elt-2* RNAi plates, and those grown on *ufd-1* RNAi were transferred to GFP+*ufd-1* and *ufd-1*+*elt-2* RNAi plates. This was followed by the incubation of the worms at 20°C for another 48 hours before transferring to *P. aeruginosa* plates. The *gfp* RNAi *E. coli* HT115(DE3) strain was a kind gift from Scott G. Kennedy, Harvard Medical School.

***C. elegans* killing assay on *P. aeruginosa* PA14**

The full-lawn killing assays of *C. elegans* on *P. aeruginosa* PA14 were carried out as described earlier (Singh and Aballay, 2019a). Briefly, *P. aeruginosa* PA14 cultures were

grown by inoculating individual bacterial colonies into 2 mL of LB broth and growing them for 8-10 hours on a shaker at 37°C. Then, 20 µL of the culture was spread on the complete surface of 3.5-cm-diameter standard slow-killing (SK) plates (modified NGM agar plates (0.35% instead of 0.25% peptone)). The plates were incubated at 37°C for 12-16 hours and then cooled to room temperature for at least 30 minutes before seeding with synchronized gravid adult hermaphrodite worms. The killing assays were performed at 25°C, and live animals were transferred to fresh plates every 24 hours. Animals were scored at the indicated times and considered dead when they failed to respond to touch. At least three independent experiments were performed for each condition.

P. aeruginosa-GFP colonization assay

The *P. aeruginosa* PA14-GFP colonization assays were carried out as described earlier (Das et al., 2023; Singh and Aballay, 2019b). Briefly, bacterial cultures were prepared by inoculating individual bacterial colonies into 2 mL of LB broth containing 50 µg/mL kanamycin and growing them for 8-10 hours on a shaker at 37°C. Then, 20 µL of the culture was spread on the complete surface of 3.5-cm-diameter SK plates containing 50 µg/mL kanamycin. The plates were incubated at 37°C for 12-16 hours and then cooled to room temperature for at least 30 min before seeding with gravid adult hermaphrodite worms. The assays were performed at 25°C. At indicated times, the worms were picked under a non-fluorescence stereomicroscope and visualized within 5 minutes under a fluorescence microscope.

Quantification of intestinal bacterial loads

The quantification of intestinal *P. aeruginosa* PA14-GFP load was carried by measuring colony-forming units (CFU) as described earlier (Das et al., 2023). Briefly, *P. aeruginosa* PA14-GFP lawns were prepared as described above. At the indicated times for each experiment, the animals were transferred from *P. aeruginosa*-GFP plates to the center of fresh *E. coli* OP50 plates thrice for 10 minutes each to eliminate bacteria stuck to their body. Afterward, ten animals/condition were transferred into 50 µL of PBS containing 0.01% triton X-100 and ground using glass beads. Serial dilutions of the lysates (10^1, 10^2, 10^3, 10^4) were seeded onto LB plates containing 50 µg/mL of kanamycin to select for *P. aeruginosa*-GFP cells and grown overnight at 37°C. Single colonies were counted the next day and represented as the number of bacterial cells or CFU per animal. Six independent experiments were performed for each condition.

Pharyngeal Pumping Assay

For the pharyngeal pumping assay without *P. aeruginosa* PA14 exposure, wild-type N2 animals were grown on appropriate RNAi clones till 1-day-old adults before the measurements. For the pharyngeal pumping assay with *P. aeruginosa* PA14 exposure, wild-type N2 animals were grown on appropriate RNAi clones till 1-day-old adults, followed by exposure to *P. aeruginosa* PA14 for 12 hours at 25°C before measurements. The number of contractions of the terminal bulb of the pharynx was counted for 30 seconds per worm. The pumping rates for at least 30 worms were recorded for each condition.

Measurement of defecation motor program (DMP) rate

The wild-type N2 animals were synchronized and grown at 20°C on EV, *ufd-1*, and *npl-4* RNAi clones till 1-day-old adults before the measurements. For the DMP assay involving exposure of *C. elegans* to *P. aeruginosa* PA14, wild-type N2 animals were synchronized and grown at 20°C on EV, *ufd-1*, and *npl-4* RNAi clones till 1-day-old adults, followed by exposure to *P. aeruginosa* PA14 for 12 hours at 25°C before measurements. The DMP cycle length was scored by assessing the time between expulsions (which are preceded by posterior and anterior body wall muscle contraction and the contraction of enteric muscles in a normal, regular pattern) (Thomas, 1990). The number of expulsion events in 15 minutes was measured for each worm. The DMP rate was recorded for 9-13worms/condition.

***C. elegans* lifespan assays**

Lifespan assays were performed as described earlier (Das et al., 2023). Briefly, the assays were performed on RNAi plates containing *E. coli* HT115(DE3) with appropriate vectors in the presence of 50 µg/mL of 5-fluorodeoxyuridine (FUdR). Animals were synchronized on RNAi plates without FUdR and incubated at 20°C. At the late L4 larval stage, the animals were transferred onto the corresponding RNAi plates containing 50 µg/mL of FUdR and incubated at 20°C. Animals were scored every day as live, dead, or gone. Animals that failed to display touch-provoked movement were scored as dead. Animals that crawled off the plates were censored. Experimental groups contained more than 60 animals per condition per replicate. Young adult animals were considered day 0 for the lifespan analysis. Three independent experiments were performed.

RNA isolation, RNA sequencing, and data analysis

RNA isolation was carried out as described earlier (Singh and Aballay, 2017). Briefly, animals were synchronized by egg laying. Approximately 35 N2 gravid adult animals were transferred to 10-cm RNAi plates seeded with control empty vector and *ufd-1* RNAi bacteria and allowed to lay eggs for 4 hours. The gravid adults were then removed, and the eggs were allowed to develop at 20°C for 96 hours. The animals were then collected, washed with M9 buffer, and frozen in TRIzol reagent (Life Technologies, Carlsbad, CA). Total RNA was extracted using the RNeasy Plus Universal Kit (Qiagen, Netherlands). Residual genomic DNA was removed using TURBO DNase (Life Technologies, Carlsbad, CA). Library preparation and sequencing were performed at the Novogene Corporation Inc, USA. The cDNA libraries were sequenced on the HiSeqX sequencing platform using 150 bp paired-end nucleotide reads.

The RNA sequence data were analyzed using the web platform Galaxy (https://usegalaxy.org/). The paired reads were first trimmed using the Trimmomatic tool. The trimmed reads obtained for each sample were mapped to the *C. elegans* genome (WS220) using the aligner STAR. The number of reads mapped to each gene was counted using the *htseq-count* tool. Differential gene expression analysis was then performed using DESeq2. Genes exhibiting at least a two-fold change and *P*-value <0.01 were considered differentially expressed. Gene ontology analysis was performed using the DAVID Bioinformatics Database (https://david.ncifcrf.gov/tools.jsp). The overlap of the upregulated genes with previously published datasets was carried out with WormExp v 2.0 (https://wormexp.zoologie.uni-kiel.de/wormexp/) (Yang et al., 2016b). The Venn diagrams were obtained using the web tool BioVenn (https://www.biovenn.nl/) (Hulsen et al., 2008).

RNA isolation and quantitative reverse transcription-PCR (qRT-PCR)

Animals were synchronized by egg laying. Approximately 40 N2 gravid adults were transferred to 9-cm RNAi plates seeded with *E. coli* HT115 expressing the appropriate vectors and allowed to lay eggs for 4 hours. The adults were then removed, and the eggs were allowed to develop at 20°C for 96 hours. The resulting animals were collected, washed with M9 buffer three times, and frozen in TRIzol reagent (Life Technologies, Carlsbad, CA). Total RNA was extracted using the RNeasy Plus Universal Kit (Qiagen, Netherlands). qRT-PCR was carried out as described earlier (Ghosh and Singh, 2024). Briefly, total RNA was reverse-transcribed with random primers using the PrimeScript™ 1st strand cDNA Synthesis Kit (TaKaRa) according to the manufacturer's protocols. qRT-PCR was conducted using TB Green fluorescence (TaKaRa) on a MasterCycler EP Realplex 4 thermal cycler (Eppendorf)

in 96-well-plate format. Fifteen microliter reactions were analyzed as outlined by the manufacturer (TaKaRa). Relative fold changes of the transcripts were calculated using the comparative *CT* ($2^{-\Delta\Delta CT}$) method and normalized to pan-actin (*act-1, -3, -4*) as previously described (Singh and Aballay, 2017). All samples were run in triplicate (technical replicates) and repeated at least four times (biological replicates).

Fluorescence imaging

Fluorescence imaging was carried out as described previously (Gokul and Singh, 2022; Ravi et al., 2023). Briefly, the animals were anesthetized using an M9 salt solution containing 50 mM sodium azide and mounted onto 2% agarose pads. The animals were then visualized using a Nikon SMZ-1000 fluorescence stereomicroscope. The fluorescence intensity was quantified using Image J software.

Quantification and statistical analysis

The statistical analysis was performed with Prism 8 (GraphPad). All error bars represent mean±standard deviation (SD). The two-sample *t*-test was used when needed, and the data were judged to be statistically significant when $P < 0.05$. In the figures, asterisks (*) denote statistical significance as follows: *, $P < 0.05$, **, $P < 0.01$, ***, $P < 0.001$, as compared with the appropriate controls. The Kaplan-Meier method was used to calculate the survival fractions, and statistical significance between survival curves was determined using the log-rank test. All experiments were performed in triplicate.

Acknowledgments

Some strains used in this study were provided by the Caenorhabditis Genetics Center (CGC), which is funded by the NIH Office of Research Infrastructure Programs (P40 OD010440).

Funding: This work was supported by the following grants: Ramalingaswami Re-entry Fellowship (Ref. No. BT/RLF/Re-entry/50/2020) and Har-Gobind Khorana-Innovative Young Biotechnologist Fellowship (File No. HRD-17011/2/2023-HRD-DBT) awarded by the Department of Biotechnology, India; STARS grant (File No. MoE-STARS/STARS-2/2023-0116) awarded by the Ministry of Education, India; Research Grant (Ref. No. 37/1741/23/EMR-II) awarded by the Council of Scientific & Industrial Research (CSIR), India; Science and Engineering Research Board (SERB) Startup (Ref. No. SRG/2020/000022) and Core (Ref. No. CRG/2023/001136) Research Grants awarded by

DST, India; and IISER Mohali intramural funds. RR was supported by a senior research fellowship from the CSIR, India.

Competing interest: The authors declare that they have no competing interest.

Data Availability: The RNA sequencing data for N2 worms grown on empty vector control and *ufd-1* RNAi have been submitted to the public repository, the Sequence Read Archive, with BioProject ID PRJNA1033335. All data generated or analyzed during this study are included in the manuscript and supporting files.

References

Amrit FRG, Naim N, Ratnappan R, Loose J, Mason C, Steenberge L, McClendon BT, Wang G, Driscoll M, Yanowitz JL, Ghazi A. 2019. The longevity-promoting factor, TCER-1, widely represses stress resistance and innate immunity. *Nat Commun* **10**:3042. doi:10.1038/s41467-019-10759-z

Bakowski MA, Desjardins CA, Smelkinson MG, Dunbar TA, Lopez-Moyado IF, Rifkin SA, Cuomo CA, Troemel ER. 2014. Ubiquitin-Mediated Response to Microsporidia and Virus Infection in C. elegans. *PLoS Pathog* **10**. doi:10.1371/journal.ppat.1004200

Bodnar NO, Rapoport TA. 2017. Molecular Mechanism of Substrate Processing by the Cdc48 ATPase Complex. *Cell* **169**:722–735. doi:10.1016/j.cell.2017.04.020

Bomberger JM, Ye S, Maceachran DP, Koeppen K, Barnaby RL, Toole GAO, Stanton BA. 2011. A Pseudomonas aeruginosa Toxin that Hijacks the Host Ubiquitin Proteolytic System. *PLoS Pathog* **7**:e1001325. doi:10.1371/journal.ppat.1001325

Boom J Van Den, Meyer H. 2018. VCP/p97-Mediated Unfolding as a Principle in Protein Homeostasis and Signaling. *Mol Cell* **69**:182–194. doi:10.1016/j.molcel.2017.10.028

Chai Q, Wang X, Qiang L, Zhang Y, Ge P, Lu Z, Zhong Y, Li B, Wang J, Zhang L, Zhou D, Li W, Dong W, Pang Y, Gao GF, Liu CH. 2019. A Mycobacterium tuberculosis surface protein recruits ubiquitin to trigger host xenophagy. *Nat Commun* **10**:1973. doi:10.1038/s41467-019-09955-8

Cheesman HK, Feinbaum RL, Thekkiniath J, Dowen RH, Conery AL, Pukkila-Worley R. 2016. Aberrant Activation of p38 MAP Kinase-Dependent Innate Immune Responses Is Toxic to Caenorhabditis elegans. *G3 (Bethesda)* **6**:541–9. doi:10.1534/g3.115.025650

Clague MJ, Urbe S. 2010. Ubiquitin: Same Molecule, Different Degradation Pathways. *Cell* **143**:682–685. doi:10.1016/j.cell.2010.11.012

Das P, Aballay A, Singh J. 2023. Calcineurin inhibition enhances Caenorhabditis elegans lifespan by defecation defects-mediated calorie restriction and nuclear hormone signaling. *Elife* **12**:RP89572.

Dikic I. 2017. Proteasomal and Autophagic Degradation Systems. *Annu Rev Biochem* **86**:193–224.

Dineen A, Osborne E, Goszczynski B, Rothman JH, Mcghee JD. 2018. Quantitating transcription factor redundancy: The relative roles of the ELT-2 and ELT-7 GATA factors in the C. elegans endoderm. *Dev Biol* **435**:150–161. doi:10.1016/j.ydbio.2017.12.023

Ding W-X, Yin X-M. 2008. Sorting, recognition and activation of the misfolded protein degradation pathways through macroautophagy and the proteasome. *Autophagy* **4**:141–150. doi:10.4161/auto.5190

Engel A, Barton GM. 2010. Unfolding new roles for XBP1 in immunity. *Nat Immunol* **11**:365–367. doi:10.1038/ni0510-365

Garcia-Sanchez JA, Ewbank JJ, Visvikis O. 2021. Ubiquitin-related processes and innate immunity in C. elegans. *Cellular and Molecular Life Sciences* **78**:4305–4333. doi:10.1007/s00018-021-03787-w

Ghosh A, Singh J. 2024. Translation initiation or elongation inhibition triggers contrasting effects on Caenorhabditis elegans survival during pathogen infection. *mBio* **15**:e0248524. doi:10.1128/mbio.02485-24

Gokul G, Singh J. 2022. Dithiothreitol causes toxicity in C. elegans by modulating the methionine-homocysteine cycle. *Elife* **11**:e76021. doi:10.7554/eLife.76021

Haldar AK, Foltz C, Finethy R, Piro AS, Feeley EM, Pilla-moffett DM, Komatsuc M, Frickelb E-M, Coers J. 2015. Ubiquitin systems mark pathogen-containing vacuoles as targets for host defense by guanylate binding proteins. *Proc Natl Acad Sci U S A* **112**:E5628–E5637. doi:10.1073/pnas.1515966112

Head B, Aballay A. 2014. Recovery from an Acute Infection in C. elegans Requires the GATA Transcription Factor ELT-2. *PLoS Genet* **10**. doi:10.1371/journal.pgen.1004609

Herhaus L, Dikic I. 2018. Regulation of Salmonella -host cell interactions via the ubiquitin system. *International Journal of Medical Microbiology* **308**:176–184. doi:10.1016/j.ijmm.2017.11.003

Hetz C, Chevet E, Oakes SA. 2015. Proteostasis control by the unfolded protein response. *Nat Cell Biol* **17**:829–838. doi:10.1038/ncb3184

Hulsen T, de Vlieg J, Alkema W. 2008. BioVenn - A web application for the comparison and visualization of biological lists using area-proportional Venn diagrams. *BMC Genomics* **9**:488. doi:10.1186/1471-2164-9-488

Husnjak K, Dikic I. 2012. Ubiquitin-Binding Proteins: Decoders of Ubiquitin- Mediated Cellular Functions. *Annu Rev Biochem* **81**:291–322. doi:10.1146/annurev-biochem-051810-094654

Kim DH, Feinbaum R, Alloing G, Emerson FE, Garsin DA, Inoue H, Tanaka-Hino M, Hisamoto N, Matsumoto K, Tan M-W, Ausubel FM. 2002. A Conserved p38 MAP

Kinase Pathway in Caenorhabditis elegans Innate Immunity. *Science (1979)* **297**:623–626. doi:10.1126/science.1073759

Kim KW, Thakur N, Piggott CA, Omi S, Polanowska J, Jin Y, Pujol N. 2016. Coordinated inhibition of C/EBP by Tribbles in multiple tissues is essential for Caenorhabditis elegans development. *BMC Biol* **14**:104. doi:10.1186/s12915-016-0320-z

Lažetić V, Blanchard MJ, Bui T, Troemel ER. 2023. Multiple pals gene modules control a balance between immunity and development in Caenorhabditis elegans. *PLoS Pathog* **19**:e1011120. doi:10.1371/journal.ppat.1011120

Lee S, Wong R, Chin C, Lim T, Eng S, Kong C, Ijap NA, Lau M-S, Lim M-P, Gan Y-H, He F-L, Tan M-W, Nathan S. 2013. Burkholderia pseudomallei suppresses Caenorhabditis elegans immunity by specific degradation of a GATA transcription factor. *Proceedings of the National Academy of Sciences* **110**:15067–15072. doi:10.1073/pnas.1311725110

Li J, Chai Q-Y, Liu CH. 2016. The ubiquitin system: a critical regulator of innate immunity and pathogen–host interactions. *Cell Mol Immunol* **13**:560–576. doi:10.1038/cmi.2016.40

Liberati NT, Fitzgerald KA, Kim DH, Feinbaum R, Golenbock DT, Ausubel FM. 2004. Requirement for a conserved Toll/interleukin-1 resistance domain protein in the Caenorhabditis elegans immune response. *Proceedings of the National Academy of Sciences* **101**:6593–6598. doi:10.1073/pnas.0308625101

Mallo G V, Le C, Couillault C, Pujol N, Granjeaud S, Kohara Y, Ewbank JJ. 2002. Inducible Antibacterial Defense System in C. elegans. *Current Biology* **12**:1209–1214.

Mann FG, Nostrand EL Van, Friedland AE, Liu X, Kim SK. 2016. Deactivation of the GATA Transcription Factor ELT-2 Is a Major Driver of Normal Aging in C. elegans. *PLoS Genet* **12**:e1005956. doi:10.1371/journal.pgen.1005956

Meng J, Fu L, Liu K, Tian C, Wu Z, Jung Y, Ferreira RB, Carroll KS, Blackwell TK, Yang J. 2021. Global profiling of distinct cysteine redox forms reveals wide-ranging redox regulation in C. elegans. *Nat Commun* **12**:1415. doi:10.1038/s41467-021-21686-3

Meyer H, Bug M, Bremer S. 2012. Emerging functions of the VCP / p97 AAA-ATPase in the ubiquitin system. *Nat Cell Biol* **14**:117–123. doi:10.1038/ncb2407

Meyer HH, Shorter JG, Seemann J, Pappin D, Warren G. 2000. A complex of mammalian Ufd1 and Npl4 links the AAA-ATPase, p97, to ubiquitin and nuclear transport pathways. *EMBO J* **19**:2181–2192. doi:10.1093/emboj/19.10.2181

Mouysset J, Deichsel A, Moser S, Hoege C, Hyman AA, Gartner A, Hoppe T. 2008. Cell cycle progression requires the CDC-48UFD-1/NPL-4 complex for efficient DNA replication. *Proc Natl Acad Sci U S A* **105**:12879–12884. doi:10.1073/pnas.0805944105

Mouysset J, Kähler C, Hoppe T. 2006. A conserved role of Caenorhabditis elegans CDC-48 in ER-associated protein degradation. *J Struct Biol* **156**:41–49. doi:10.1016/j.jsb.2006.02.015

Mukhopadhyay D, Riezman H. 2007. Proteasome-Independent Functions of Ubiquitin in Endocytosis and Signaling. *Science (1979)* **315**:201–205.

Olaitan AO, Aballay A. 2018. Non-proteolytic activity of 19S proteasome subunit RPT-6 regulates GATA transcription during response to infection. *PLoS Genet* **14**:e1007693.

Otarigho B, Aballay A. 2021. Immunity-longevity tradeoff neurally controlled by GABAergic transcription factor PITX1/UNC-30. *Cell Rep* **35**:109187. doi:10.1016/j.celrep.2021.109187

Otten EG, Werner E, Crespillo-casado A, Boyle KB, Dharamdasani V, Pathe C, Santhanam B, Randow F. 2021. Ubiquitylation of lipopolysaccharide by RNF213 during bacterial infection. *Nature* **594**:111–116. doi:10.1038/s41586-021-03566-4

Peterson ND, Icso JD, Salisbury JE, Rodríguez T, Thompson PR, Pukkila-Worley R. 2022. Pathogen infection and cholesterol deficiency activate the C. elegans p38 immune pathway through a TIR-1/SARM1 phase transition. *Elife* **11**:e74206.

Ravi, Kumar A, Bhattacharyya S, Singh J. 2023. Thiol reductive stress activates the hypoxia response pathway. *EMBO J* **42**:e114093. doi:10.15252/embj.2023114093

Reddy KC, Dror T, Underwood RS, Osman GA, Elder CR, Desjardins CA, Cuomo CA, Barkoulas M, Troemel ER. 2019. Antagonistic paralogs control a switch between growth and pathogen resistance in C. elegans. *PLoS Pathog* **15**:e1007528. doi:10.1371/journal.ppat.1007528

Ren Z, Ambros VR. 2015. Caenorhabditis elegans microRNAs of the let-7 family act in innate immune response circuits and confer robust developmental timing against pathogen stress. *Proc Natl Acad Sci U S A* **112**:E2366–E2375. doi:10.1073/pnas.1422858112

Ribet D, Cossart P. 2018. Ubiquitin, SUMO, and NEDD8: Key Targets of Bacterial Pathogens. *Trends Cell Biol* **28**:926–940. doi:10.1016/j.tcb.2018.07.005

Richardson CE, Kooistra T, Kim DH. 2010. An essential role for XBP-1 in host protection against immune activation in C. elegans. *Nature* **463**:1092–1095. doi:10.1038/nature08762

Sarkies P, Ashe A, Pen J Le, Mckie MA, Miska EA. 2013. Competition between virus-derived and endogenous small RNAs regulates gene expression in Caenorhabditis elegans. *Genome Res* **23**:1258–1270. doi:10.1101/gr.153296.112

Sasagawa Y, Yamanaka K, Ogura T. 2007. ER E3 ubiquitin ligase HRD-1 and its specific partner chaperone BiP play important roles in ERAD and developmental growth in Caenorhabditis elegans. *Genes to Cells* **12**:1063–1073. doi:10.1111/j.1365-2443.2007.01108.x

Shapira M, Hamlin BJ, Rong J, Chen K, Ronen M, Tan M-W. 2006. A conserved role for a GATA transcription factor in regulating epithelial innate immune responses. *Proc Natl Acad Sci U S A* **103**:14086–91. doi:10.1073/pnas.0603424103

Singh J. 2023. ERASing endoplasmic reticulum stress: the faster, the better. *Trends Cell Biol* **33**:179–181. doi:10.1016/j.tcb.2022.12.003

Singh J, Aballay A. 2020. Neural control of behavioral and molecular defenses in C. elegans. *Curr Opin Neurobiol* **62**:34–40. doi:10.1016/j.conb.2019.10.012

Singh J, Aballay A. 2019a. Intestinal infection regulates behavior and learning via neuroendocrine signaling. *Elife* **8**:e50033. doi:10.7554/eLife.50033

Singh J, Aballay A. 2019b. Microbial colonization activates an immune fight-and-flight response via neuroendocrine signaling. *Dev Cell* **49**:89–99. doi:10.1016/j.devcel.2019.02.001

Singh J, Aballay A. 2017. Endoplasmic reticulum stress caused by lipoprotein accumulation suppresses immunity against bacterial pathogens and contributes to immunosenescence. *mBio* **8**:e00778-17. doi:10.1128/mBio.00778-17

Sun J, Liu Y, Aballay A. 2012. Organismal regulation of XBP-1-mediated unfolded protein response during development and immune activation. *EMBO Rep* **13**:855–860. doi:10.1038/embor.2012.100

Tan MW, Mahajan-Miklos S, Ausubel FM. 1999. Killing of Caenorhabditis elegans by Pseudomonas aeruginosa used to model mammalian bacterial pathogenesis. *Proc Natl Acad Sci U S A* **96**:715–20. doi:10.1073/pnas.96.2.715

Taylor RC, Dillin A. 2013. XBP-1 Is a cell-nonautonomous regulator of stress resistance and longevity. *Cell* **153**:1435–1447. doi:10.1016/j.cell.2013.05.042

Thomas JH. 1990. Genetic analysis of defecation in Caenorhabditis elegans. *Genetics* **124**:855–872. doi:10.1016/0168-9525(90)90166-4

Tripathi-Giesgen I, Behrends C, Alpi AF. 2021. The ubiquitin ligation machinery in the defense against bacterial pathogens. *EMBO Rep* **22**:e52864. doi:10.15252/embr.202152864

Vembar SS, Brodsky JL. 2008. One step at a time: endoplasmic reticulum-associated degradation. *Nat Rev Mol Cell Biol* **9**:944–957. doi:10.1038/nrm2546

Vilchez D, Saez I, Dillin A. 2014. The role of protein clearance mechanisms in organismal ageing and age-related diseases. *Nat Commun* **5**:5659. doi:10.1038/ncomms6659

Visvikis O, Ihuegbu N, Labed SA, Luhachack LG, Alves AMF, Wollenberg AC, Stuart LM, Stormo GD, Irazoqui JE. 2014. Innate host defense requires TFEB-mediated transcription of cytoprotective and antimicrobial genes. *Immunity* **40**:896–909. doi:10.1016/j.immuni.2014.05.002

Wolf DH, Stolz A. 2012. The Cdc48 machine in endoplasmic reticulum associated protein degradation ☆. *Biochim Biophys Acta* **1823**:117–124. doi:10.1016/j.bbamcr.2011.09.002

Wu X, Rapoport TA. 2018. Mechanistic insights into ER-associated protein degradation. *Curr Opin Cell Biol* **53**:22–28. doi:10.1016/j.ceb.2018.04.004

Yang W, Dierking K, Rosenstiel PC, Schulenburg H. 2016a. GATA transcription factor as a likely key regulator of the Caenorhabditis elegans innate immune response against gut pathogens. *Zoology* **119**:244–253. doi:10.1016/j.zool.2016.05.013

Yang W, Dierking K, Schulenburg H. 2016b. WormExp: A web-based application for a Caenorhabditis elegans-specific gene expression enrichment analysis. *Bioinformatics* **32**:943–945. doi:10.1093/bioinformatics/btv667

Ye Y, Meyer HH, Rapoport TA. 2001. The AAA ATPase Cdc48/p97 and its partners transport proteins from the ER into the cytosol. *Nature* **414**:652–656.

Figures

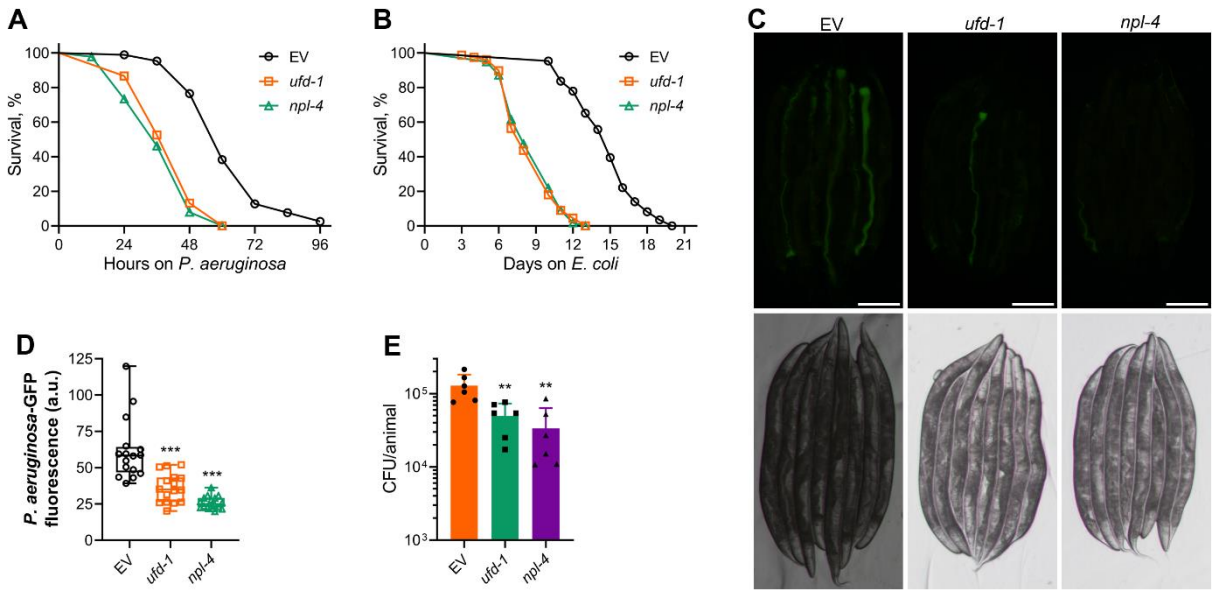

Figure 1. Inhibition of the UFD-1-NPL-4 complex reduces survival of *C. elegans* on *P. aeruginosa*

(A) Representative survival plots of N2 animals on *P. aeruginosa* PA14 at 25°C after treatment with the empty vector (EV) control, *ufd-1*, and *npl-4* RNAi. $P < 0.001$ for *ufd-1* and *npl-4* RNAi compared to EV control.

(B) Representative survival plots of N2 animals grown on bacteria for RNAi against *ufd-1* and *npl-4*, along with the EV control at 20°C. Day 0 represents young adults. $P < 0.001$ for *ufd-1* and *npl-4* RNAi compared to EV control.

(C) Representative fluorescence (top) and the corresponding brightfield (bottom) images of N2 animals incubated on *P. aeruginosa*-GFP for 24 hours at 25°C after growth on the EV control, *ufd-1*, and *npl-4* RNAi bacteria. Scale bar = 200 µm.

(D) Quantification of GFP levels of N2 animals incubated on *P. aeruginosa*-GFP for 24 hours at 25°C after growth on the EV control, *ufd-1*, and *npl-4* RNAi bacteria. ***$P < 0.001$ via the *t*-test ($n = 16$ worms each).

(E) Colony-forming units (CFU) per animal of N2 worms incubated on *P. aeruginosa*-GFP for 24 hours at 25°C after growth on the EV control, *ufd-1*, and *npl-4* RNAi bacteria. **$P < 0.01$ via the *t*-test (n = 6 biological replicates).

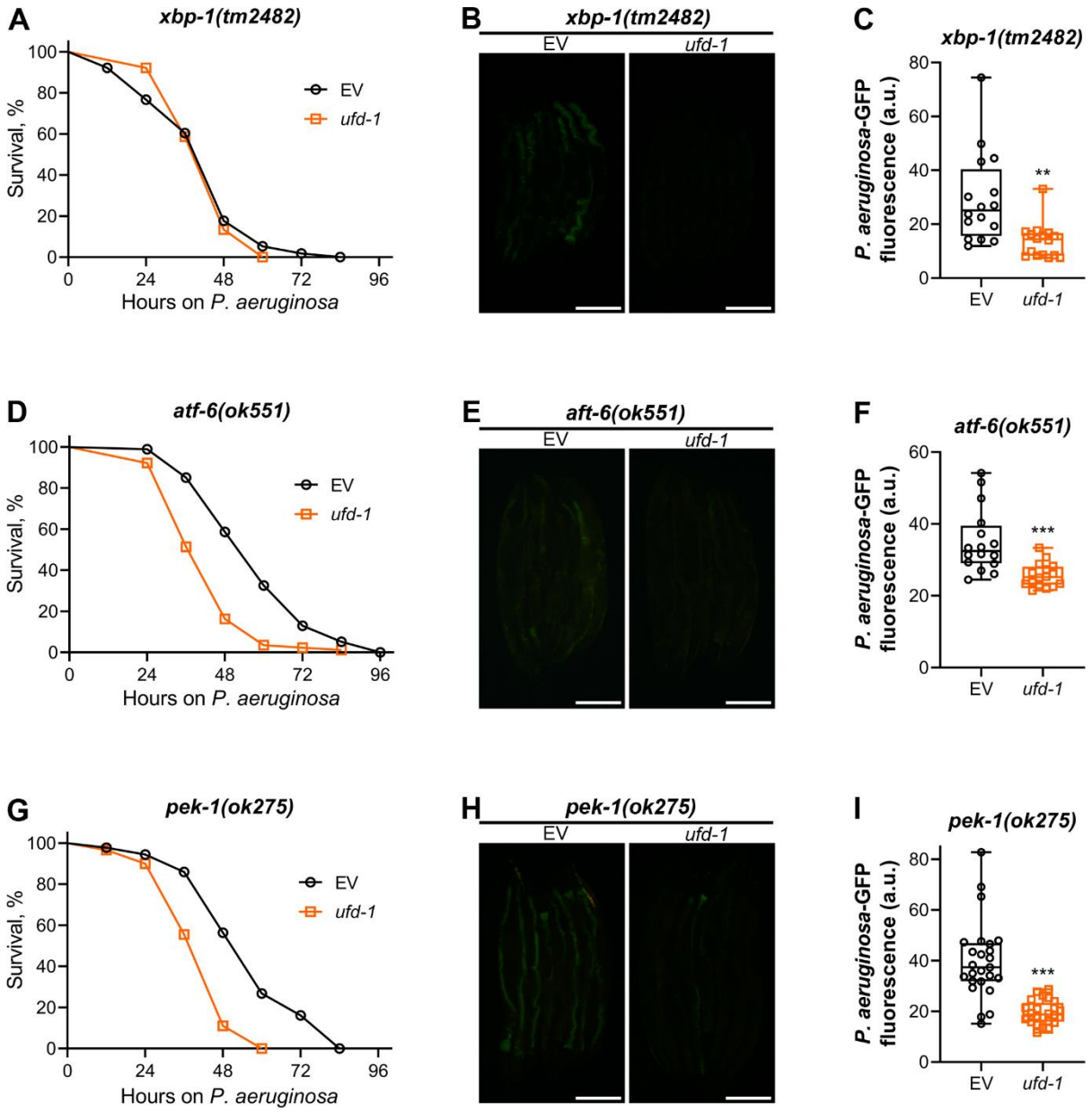

Figure 2. Reduced colonization with *P. aeruginosa* upon *ufd-1* knockdown is independent of the ER-UPR pathways

(A) Representative survival plots of *xbp-1(tm2482)* animals on *P. aeruginosa* PA14 at 25°C after treatment with the empty vector (EV) control and *ufd-1* RNAi. The difference between the EV and *ufd-1* RNAi survival plots is nonsignificant.

(B) Representative fluorescence images of *xbp-1(tm2482)* animals incubated on *P. aeruginosa*-GFP for 24 hours at 25°C after growth on the EV control and *ufd-1* RNAi bacteria. Scale bar = 200 µm.

(C) Quantification of GFP levels of *xbp-1(tm2482)* animals incubated on *P. aeruginosa*-GFP for 24 hours at 25°C after growth on the EV control and *ufd-1* RNAi bacteria. $^{**}P < 0.01$ via the *t*-test ($n = 16$ worms each).

(D) Representative survival plots of *atf-6(ok551)* animals on *P. aeruginosa* PA14 at 25°C after treatment with the EV control and *ufd-1* RNAi. $P < 0.001$.

(E) Representative fluorescence images of *atf-6(ok551)* animals incubated on *P. aeruginosa*-GFP for 24 hours at 25°C after growth on the EV control and *ufd-1* RNAi bacteria. Scale bar = 200 μm.

(F) Quantification of GFP levels of *atf-6(ok551)* animals incubated on *P. aeruginosa*-GFP for 24 hours at 25°C after growth on the EV control and *ufd-1* RNAi bacteria. $^{***}P < 0.001$ via the *t*-test ($n = 16$ worms each).

(G) Representative survival plots of *pek-1(ok275)* animals on *P. aeruginosa* PA14 at 25°C after treatment with the EV control and *ufd-1* RNAi. $P < 0.001$.

(H) Representative fluorescence images of *pek-1(ok275)* animals incubated on *P. aeruginosa*-GFP for 24 hours at 25°C after growth on the EV control and *ufd-1* RNAi bacteria. Scale bar = 200 μm.

(I) Quantification of GFP levels of *pek-1(ok275)* animals incubated on *P. aeruginosa*-GFP for 24 hours at 25°C after growth on the EV control and *ufd-1* RNAi bacteria. $^{***}P < 0.001$ via the *t*-test ($n = 24$–25 worms each).

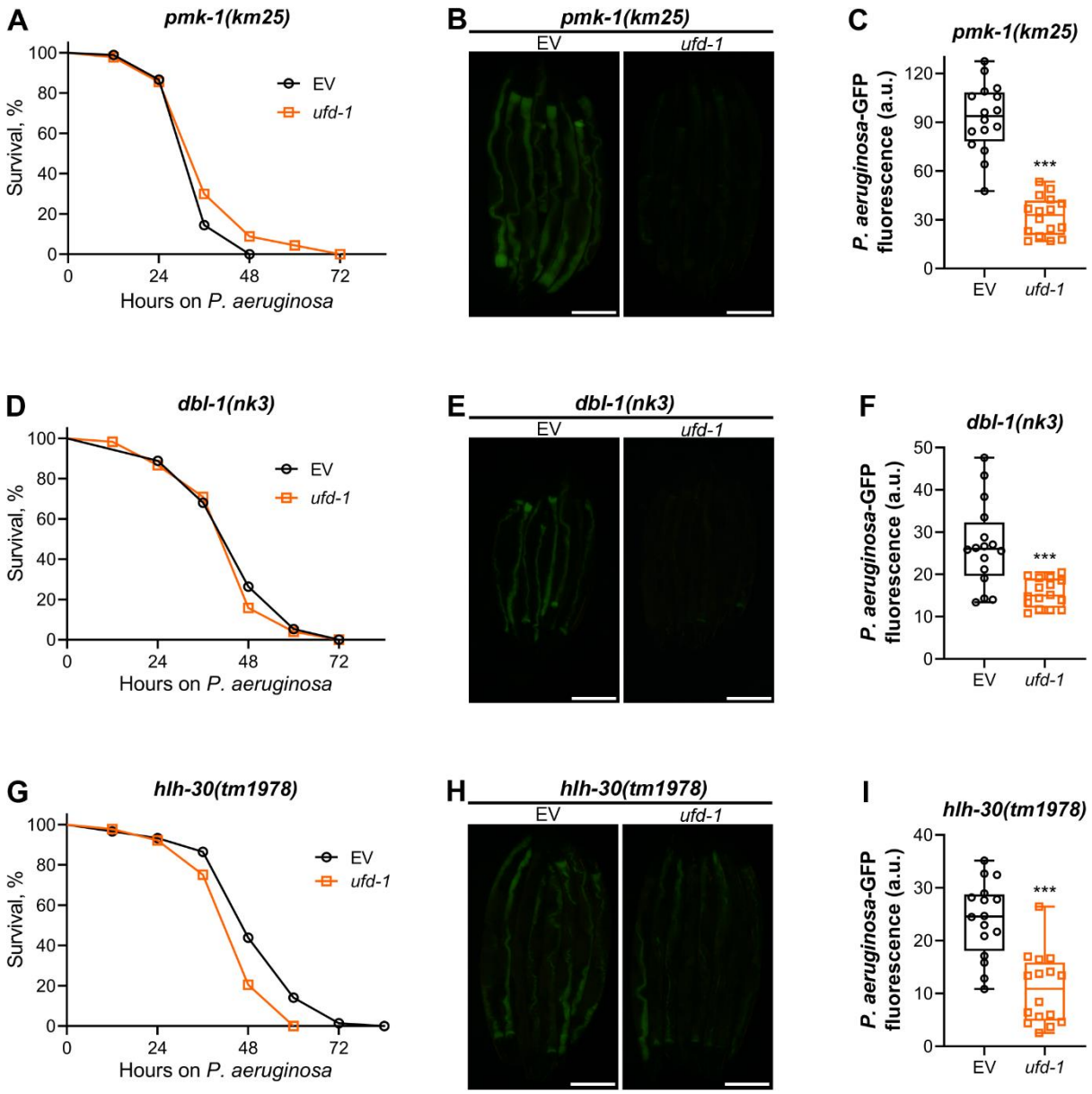

Figure 3. Reduced colonization with *P. aeruginosa* upon *ufd-1* knockdown is independent of the major immunity pathways

(A) Representative survival plots of *pmk-1(km25)* animals on *P. aeruginosa* PA14 at 25°C after treatment with the empty vector (EV) control and *ufd-1* RNAi. The difference between the EV and *ufd-1* RNAi survival plots is nonsignificant.

(B) Representative fluorescence images of *pmk-1(km25)* animals incubated on *P. aeruginosa*-GFP for 24 hours at 25°C after growth on the EV control and *ufd-1* RNAi bacteria. Scale bar = 200 µm.

(C) Quantification of GFP levels of *pmk-1(km25)* animals incubated on *P. aeruginosa*-GFP for 24 hours at 25°C after growth on the EV control and *ufd-1* RNAi bacteria. ***$P < 0.001$ via the *t*-test ($n = 16$ worms each).

(D) Representative survival plots of *dbl-1(nk3)* animals on *P. aeruginosa* PA14 at 25°C after treatment with the EV control and *ufd-1* RNAi. The difference between the EV and *ufd-1* RNAi survival plots is nonsignificant.

(E) Representative fluorescence images of *dbl-1(nk3)* animals incubated on *P. aeruginosa*-GFP for 24 hours at 25°C after growth on the EV control and *ufd-1* RNAi bacteria. Scale bar = 200 μm.

(F) Quantification of GFP levels of *dbl-1(nk3)* animals incubated on *P. aeruginosa*-GFP for 24 hours at 25°C after growth on the EV control and *ufd-1* RNAi bacteria. ***$P < 0.001$ via the *t*-test ($n = 16$ worms each).

(G) Representative survival plots of *hlh-30(tm1978)* animals on *P. aeruginosa* PA14 at 25°C after treatment with the EV control and *ufd-1* RNAi. $P < 0.001$.

(H) Representative fluorescence images of *hlh-30(tm1978)* animals incubated on *P. aeruginosa*-GFP for 24 hours at 25°C after growth on the EV control and *ufd-1* RNAi bacteria. Scale bar = 200 μm.

(I) Quantification of GFP levels of *hlh-30(tm1978)* animals incubated on *P. aeruginosa*-GFP for 24 hours at 25°C after growth on the EV control and *ufd-1* RNAi bacteria. ***$P < 0.001$ via the *t*-test ($n = 16$ worms each).

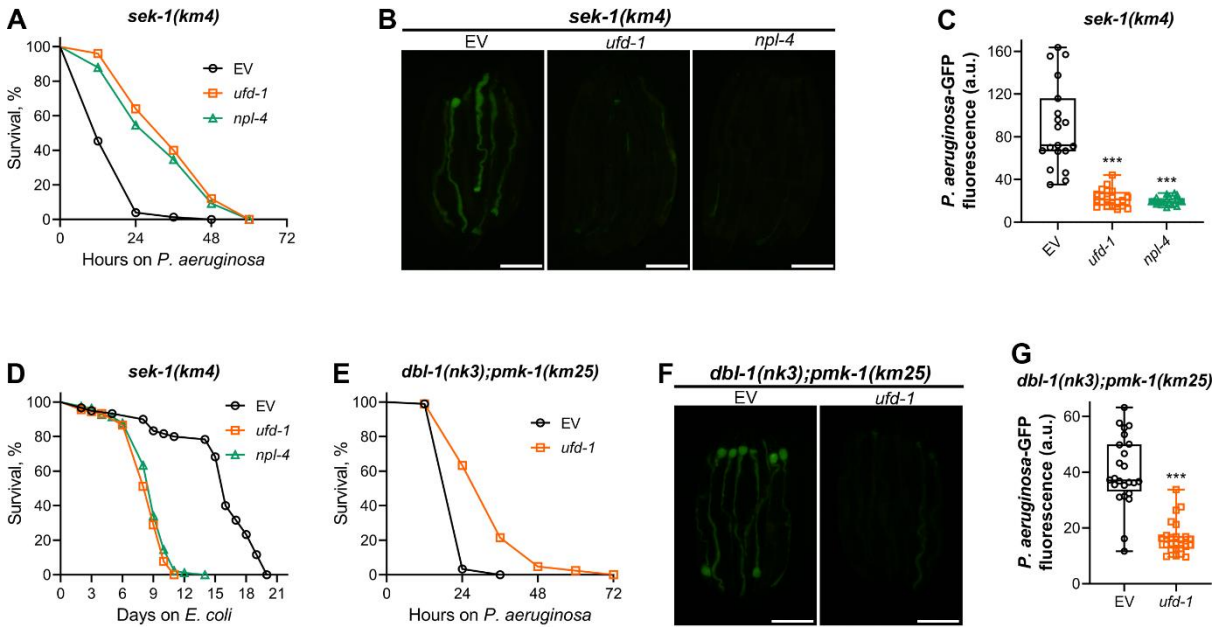

Figure 4. Inhibition of the UFD-1-NPL-4 complex improves survival of severely immunocompromised *C. elegans* on *P. aeruginosa*

(A) Representative survival plots of *sek-1(km4)* animals on *P. aeruginosa* PA14 at 25°C after treatment with the empty vector (EV) control, *ufd-1*, and *npl-4* RNAi. $P < 0.001$ for *ufd-1* and *npl-4* RNAi compared to EV control.

(B) Representative fluorescence images of *sek-1(km4)* animals incubated on *P. aeruginosa*-GFP for 12 hours at 25°C after growth on the EV control, *ufd-1*, and *npl-4* RNAi bacteria. Scale bar = 200 µm.

(C) Quantification of GFP levels of *sek-1(km4)* animals incubated on *P. aeruginosa*-GFP for 12 hours at 25°C after growth on the EV control, *ufd-1*, and *npl-4* RNAi bacteria. ***$P < 0.001$ via the *t*-test (n = 19–20 worms each).

(D) Representative survival plots of *sek-1(km4)* animals grown on bacteria for RNAi against *ufd-1* and *npl-4* along with the EV control at 20°C. Day 0 represents young adults. $P < 0.001$ for *ufd-1* and *npl-4* RNAi compared to EV control.

(E) Representative survival plots of *dbl-1(nk3);pmk-1(km25)* animals on *P. aeruginosa* PA14 at 25°C after treatment with the EV control and *ufd-1* RNAi. $P < 0.001$.

(F) Representative fluorescence images of *dbl-1(nk3);pmk-1(km25)* animals incubated on *P. aeruginosa*-GFP for 12 hours at 25°C after growth on the EV control and *ufd-1* RNAi bacteria. Scale bar = 200 µm.

(G) Quantification of GFP levels of *dbl-1(nk3);pmk-1(km25)* animals incubated on *P. aeruginosa*-GFP for 12 hours at 25°C after growth on the EV control and *ufd-1* RNAi bacteria. ***$P < 0.001$ via the *t*-test ($n = 24$ worms each).

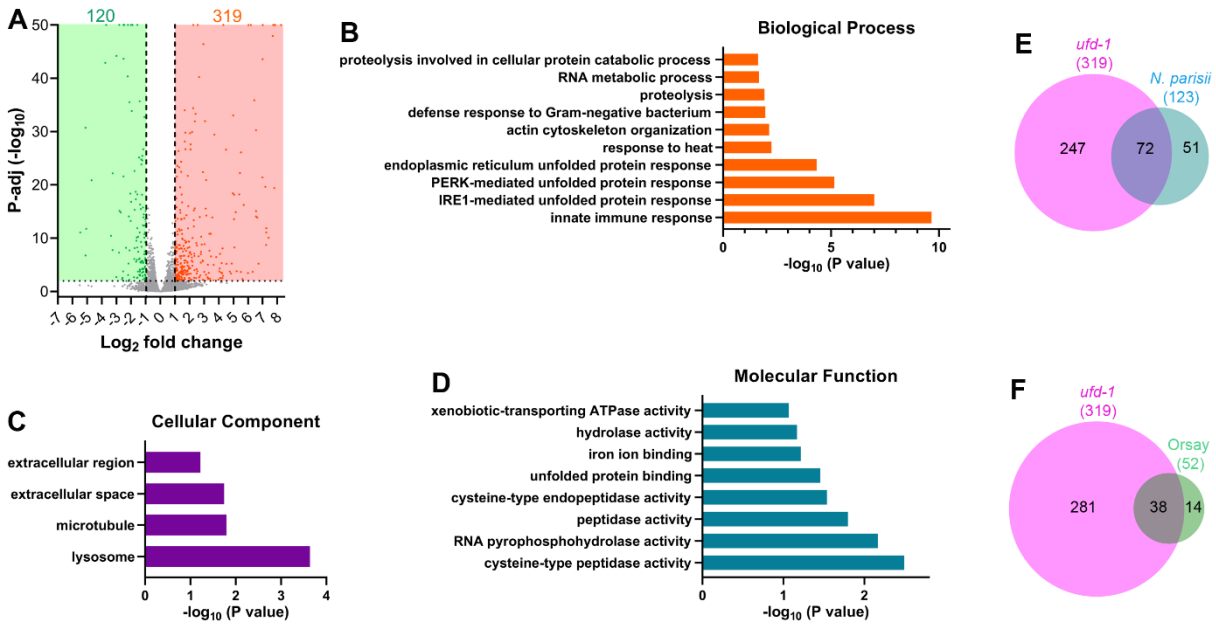

Figure 5. Knockdown of *ufd-1* results in the upregulation of protease and intracellular pathogen response genes

(A) Volcano plot of upregulated and downregulated genes in *ufd-1* RNAi versus empty vector (EV) control RNAi N2 animals. Orange and green dots represent significantly upregulated and downregulated genes, respectively, while the grey dots represent the genes that are not differentially regulated.

(B)-(D) Gene ontology enrichment analysis for *ufd-1* RNAi upregulated genes for biological processes (B), cellular component (C), and molecular function (D).

(E) Venn diagram showing the overlap between genes upregulated upon *ufd-1* RNAi and upregulated upon *Nematocida parisii* infection (Bakowski et al., 2014). The *P*-value for the overlap between the data is 8.2×10^{-110}.

(F) Venn diagram showing the overlap between genes upregulated upon *ufd-1* RNAi and upregulated upon Orsay virus infection (Sarkies et al., 2013). The *P*-value for the overlap between the data is 2.7×10^{-62}.

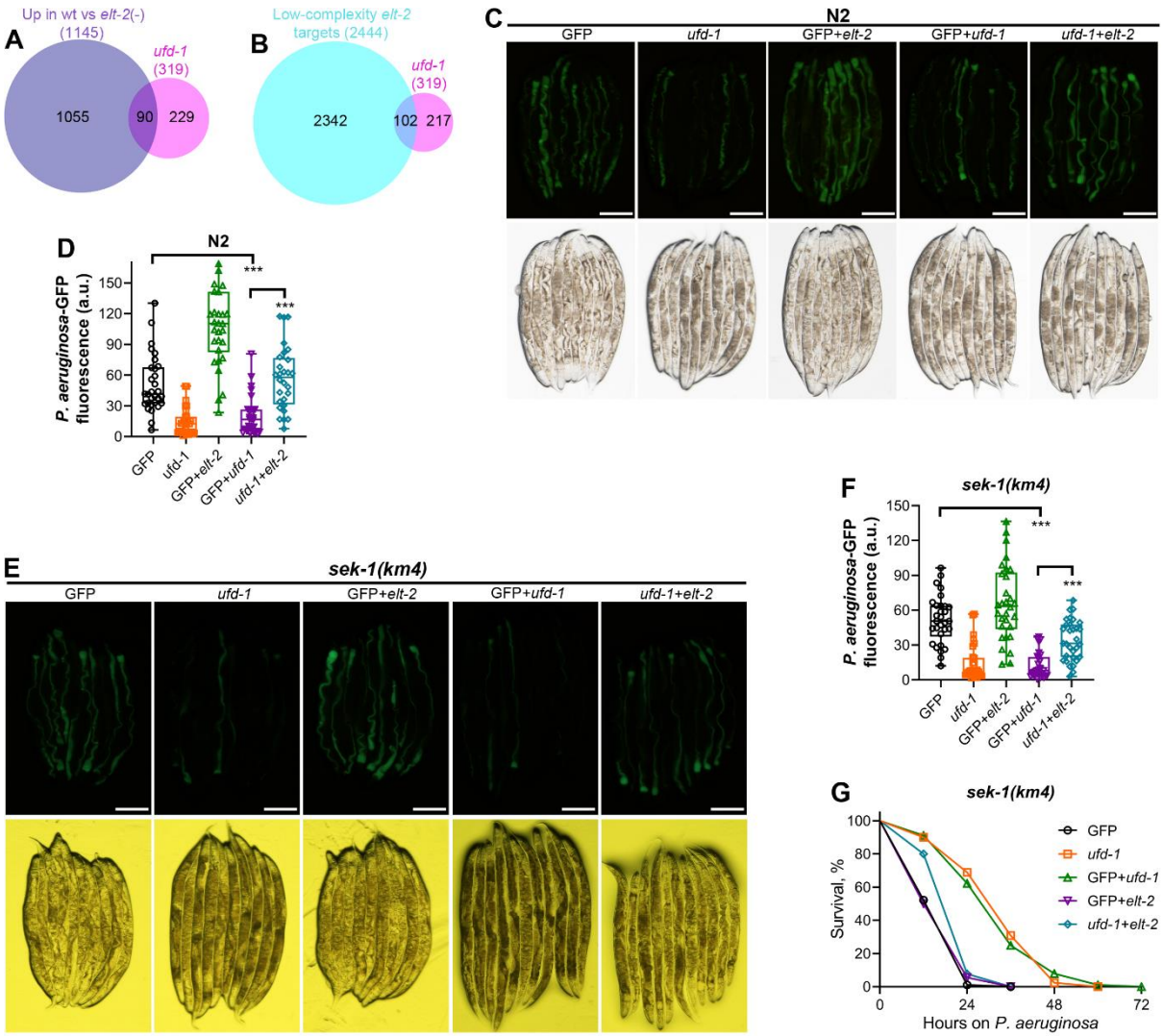

Figure 6. GATA transcription factor ELT-2 mediates the *ufd-1* knockdown phenotypes

(A) Venn diagram showing the overlap between genes upregulated upon *ufd-1* RNAi and upregulated in wt versus *elt-2*(-) larvae (Dineen et al., 2018). The *P*-value for the overlap between the data is 9.5×10^{-52}.

(B) Venn diagram showing the overlap between genes upregulated upon *ufd-1* RNAi and the low-complexity ELT-2 target genes (Mann et al., 2016). The *P*-value for the overlap between the data is 1.5×10^{-34}.

(C) Representative fluorescence (top) and the corresponding brightfield (bottom) images of N2 animals incubated on *P. aeruginosa*-GFP for 24 hours at 25°C after growth on the *gfp* RNAi (GFP) control, *ufd-1*, GFP+*elt-2*, GFP+*ufd-1*, and *ufd-1*+*elt-2* RNAi bacteria (see Methods for the details). Scale bar = 200 μm.

(D) Quantification of GFP levels of N2 animals incubated on *P. aeruginosa*-GFP for 24 hours at 25°C after growth on the *gfp* RNAi control, *ufd-1*, GFP+*elt-2*, GFP+*ufd-1*, and *ufd-1*+*elt-2* RNAi bacteria. ***$P < 0.001$ via the *t*-test ($n = 28$-30 worms each).

(E) Representative fluorescence (top) and the corresponding brightfield (bottom) images of *sek-1(km4)* animals incubated on *P. aeruginosa*-GFP for 12 hours at 25°C after growth on the *gfp* RNAi control, *ufd-1*, GFP+*elt-2*, GFP+*ufd-1*, and *ufd-1*+*elt-2* RNAi bacteria. Scale bar = 200 μm.

(F) Quantification of GFP levels of *sek-1(km4)* animals incubated on *P. aeruginosa*-GFP for 12 hours at 25°C after growth on the *gfp* RNAi control, *ufd-1*, GFP+*elt-2*, GFP+*ufd-1*, and *ufd-1*+*elt-2* RNAi bacteria. ***$P < 0.001$ via the *t*-test ($n = 30$-31 worms each).

(G) Representative survival plots of *sek-1(km4)* animals on *P. aeruginosa* PA14 at 25°C after treatment with the *gfp* RNAi control, *ufd-1*, GFP+*elt-2*, GFP+*ufd-1*, and *ufd-1*+*elt-2* RNAi bacteria. $P < 0.001$ for *ufd-1*+*elt-2* RNAi compared to GFP+*ufd-1* RNAi.

Supplementary Figures

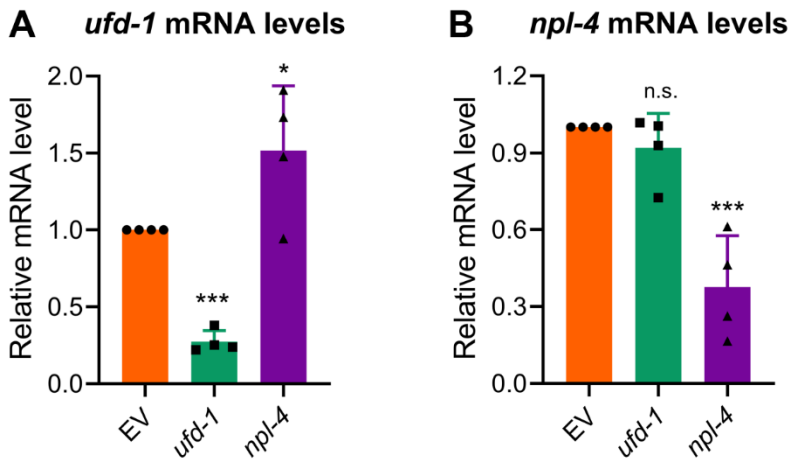

Figure 1—figure supplement 1. RNAi against *ufd-1* and *npl-4* results in the specific knockdown of their corresponding mRNAs

(A)-(B) Quantitative reverse transcription-PCR for *ufd-1* mRNA (A) and *npl-4* mRNA (B) levels in N2 animals grown on the empty vector (EV) control, *ufd-1*, and *npl-4* RNAi bacteria at 20 °C until 1-day-old adults. ***$P < 0.001$ and *$P < 0.05$ via the *t*-test. n.s., nonsignificant (n = 4 biological replicates).

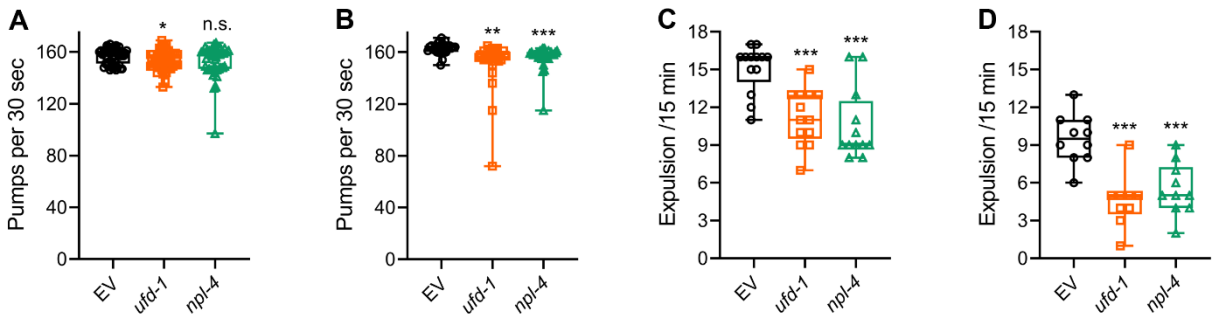

Figure 1—figure supplement 2. Effects on pharyngeal pumping and defecation are unlikely to be the reason for reduced pathogen colonization upon inhibition of the UFD-1-NPL-4 complex

(A) Pharyngeal pumps per 30 seconds of N2 animals grown on *ufd-1* and *npl-4* RNAi, along with the empty vector (EV) control RNAi. $*P < 0.05$ via the *t*-test. n.s., nonsignificant ($n = 45$ worms each).

(B) Pharyngeal pumps per 30 seconds of N2 animals grown on EV control, *ufd-1*, and *npl-4* RNAi, followed by incubation on *P. aeruginosa* PA14 at 25°C for 12 hours. $***P < 0.001$ and $**P < 0.01$ via the *t*-test ($n = 30$ worms each).

(C) The number of expulsion events observed in 15 minutes in N2 animals grown on EV control, *ufd-1*, and *npl-4* RNAi. $***P < 0.001$ via the *t*-test. ($n = 12$-13 worms each).

(D) The number of expulsion events observed in 15 minutes in N2 animals grown on EV control, *ufd-1*, and *npl-4* RNAi, followed by incubation on *P. aeruginosa* PA14 at 25°C for 12 hours. $***P < 0.001$ via the *t*-test. ($n = 9$-10 worms each).

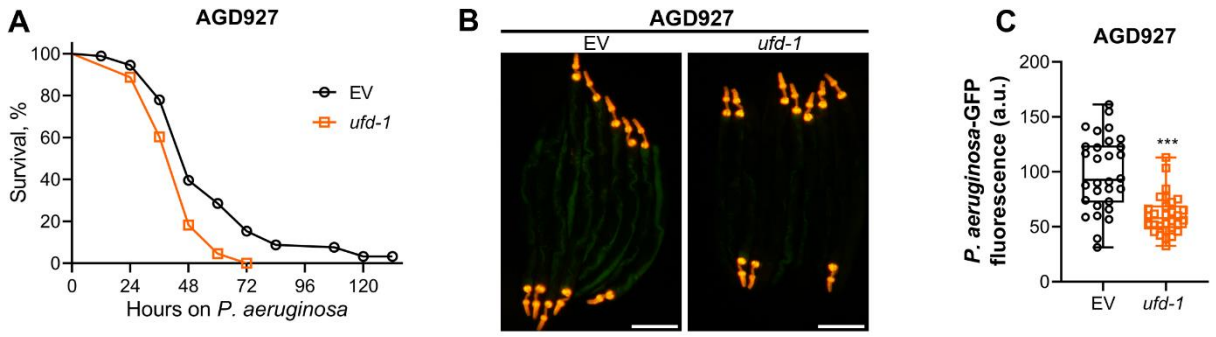

Figure 2—figure supplement 1. Reduced colonization with *P. aeruginosa* upon *ufd-1* knockdown is independent of the XBP-1 ER-UPR pathway

(A) Representative survival plots of AGD927 (neuronally overexpressing the constitutively active spliced form of XBP-1, XBP-1s) animals on *P. aeruginosa* PA14 at 25°C after treatment with the empty vector (EV) control and *ufd-1* RNAi. $P < 0.001$.

(B) Representative fluorescence images of AGD927 animals incubated on *P. aeruginosa*-GFP for 24 hours at 25°C after growth on the EV control and *ufd-1* RNAi bacteria. The red fluorescence in the pharynx region is from the *myo-2p::tdTomato* coinjection marker. Scale bar = 200 µm.

(C) Quantification of GFP levels of AGD927 animals incubated on *P. aeruginosa*-GFP for 24 hours at 25°C after growth on the EV control and *ufd-1* RNAi bacteria. ***$P < 0.001$ via the *t*-test ($n = 30$ worms each).

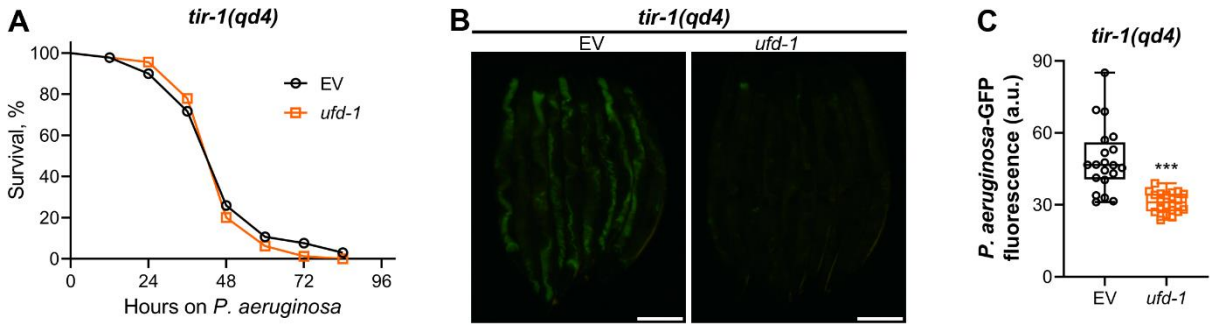

Figure 3—figure supplement 1. Reduced gut colonization upon *ufd-1* knockdown is independent of the *tir-1* immunity pathway

(A) Representative survival plots of *tir-1(qd4)* animals on *P. aeruginosa* PA14 at 25°C after treatment with the empty vector (EV) control and *ufd-1* RNAi. The difference between the EV and *ufd-1* RNAi survival plots is nonsignificant.

(B) Representative fluorescence images of *tir-1(qd4)* animals incubated on *P. aeruginosa*-GFP for 24 hours at 25°C after growth on the EV control and *ufd-1* RNAi bacteria. Scale bar = 200 μm.

(C) Quantification of GFP levels of *tir-1(qd4)* animals incubated on *P. aeruginosa*-GFP for 24 hours at 25°C after growth on the EV control and *ufd-1* RNAi bacteria. ***$P < 0.001$ via the *t*-test (n = 19-20 worms each).

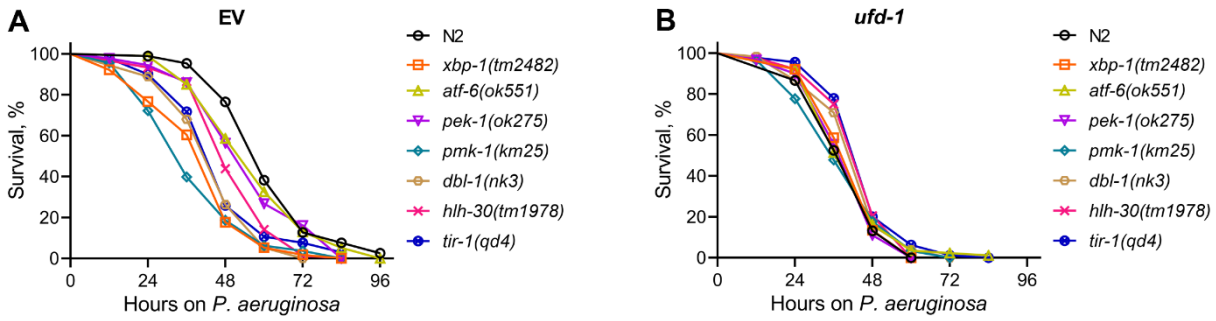

Figure 4—figure supplement 1. Knockdown of *ufd-1* dictates survival of different worm strains on *P. aeruginosa*

(A) Representative survival plots of worm strains on *P. aeruginosa* PA14 at 25°C after treatment with the empty vector (EV) control RNAi.

(B) Representative survival plots of worm strains on *P. aeruginosa* PA14 at 25°C after treatment with *ufd-1* RNAi.

The data in (A) and (B) are pooled from the data from Figures 1-3 and Figure 3—figure supplement 1.

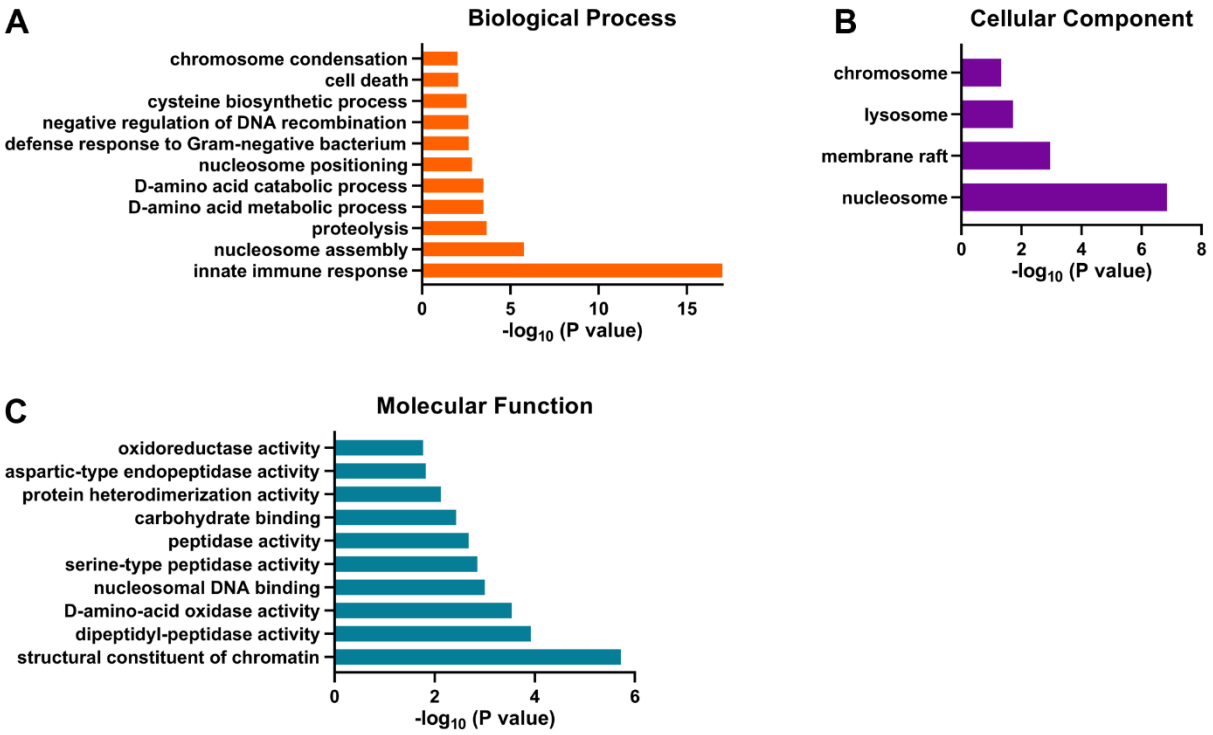

Figure 5—figure supplement 1. Gene ontology enrichment analysis for *ufd-1* RNAi downregulated genes

(A)-(C) Gene ontology enrichment analysis for *ufd-1* RNAi downregulated genes for biological processes (A), cellular component (B), and molecular function (C).

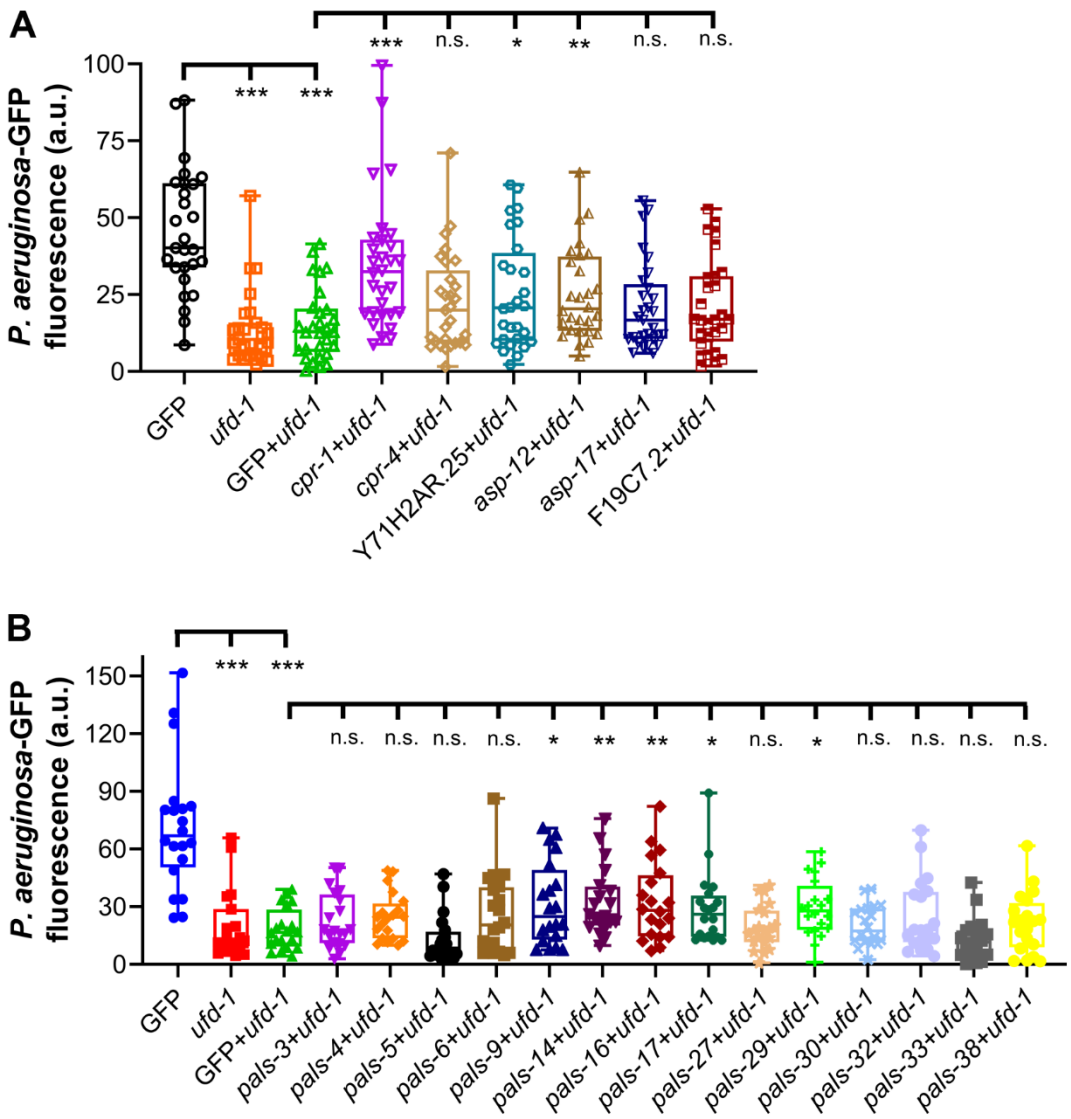

Figure 6—figure supplement 1. Role of protease or intracellular pathogen response genes in reduced colonization of *ufd-1* RNAi animals

(A) Quantification of GFP levels of N2 animals incubated on *P. aeruginosa*-GFP for 24 hours at 25°C after growth on indicated RNAi bacteria. *P*-values in comparison to the *gfp* RNAi (GFP) and GFP+*ufd-1* RNAi are indicated. ***$P < 0.001$, **$P < 0.01$, and *$P < 0.05$ via the *t*-test. n.s., nonsignificant ($n = 26$-30 worms each).

(B) Quantification of GFP levels of N2 animals incubated on *P. aeruginosa*-GFP for 24 hours at 25°C after growth on indicated RNAi bacteria. *P*-values in comparison to the *gfp* RNAi (GFP) and GFP+*ufd-1* RNAi are indicated. ***$P < 0.001$, **$P < 0.01$, and *$P < 0.05$ via the *t*-test. n.s., nonsignificant ($n = 19$-20 worms each).

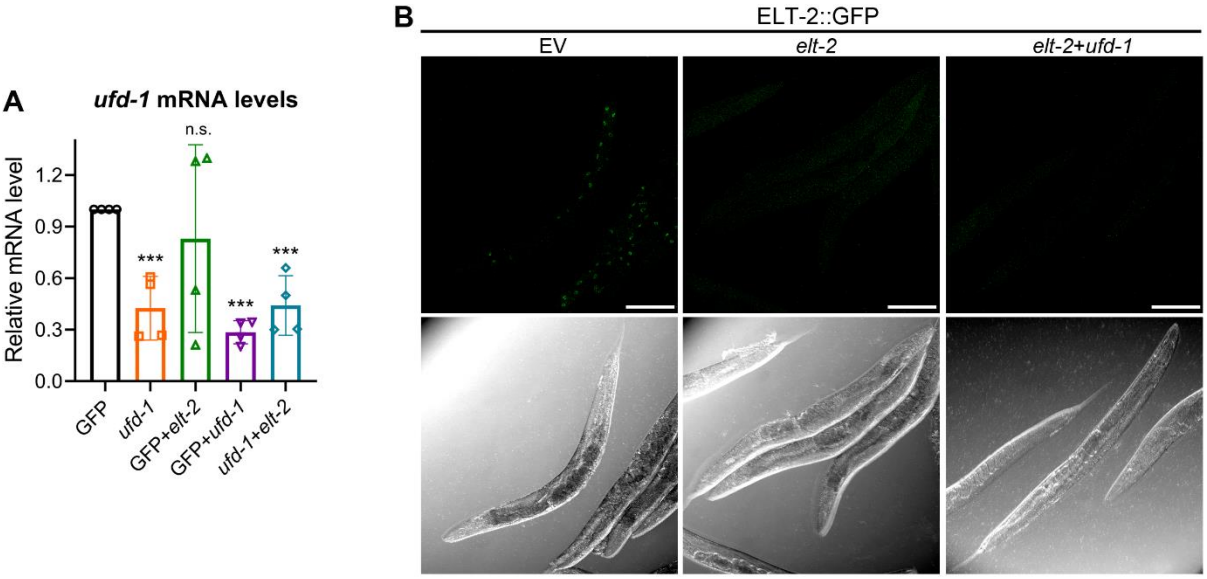

Figure 6—figure supplement 2. Double RNAi does not impact *ufd-1* or *elt-2* mRNA knockdown

(A) Quantitative reverse transcription-PCR for *ufd-1* mRNA levels in N2 animals grown on the *gfp* RNAi control (GFP), *ufd-1*, GFP+*elt-2*, GFP+*ufd-1*, and *ufd-1*+*elt-2* RNAi bacteria. ***$P < 0.001$ via the *t*-test. n.s., nonsignificant (n = 4 biological replicates).

(B) Representative fluorescence and corresponding brightfield images of ELT-2::GFP worms grown on the control empty vector (EV), *elt-2*, and *elt-2*+*ufd-1* RNAi bacteria. Scale bar = 200 µm.

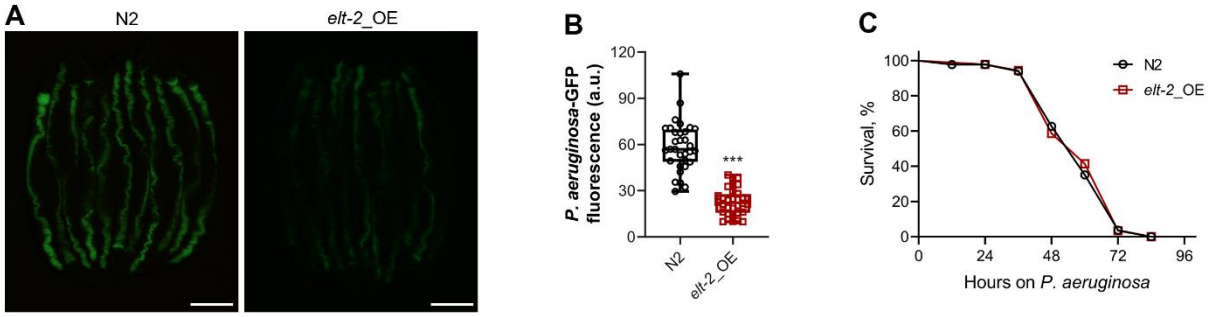

Figure 6—figure supplement 3. ELT-2 overexpression partly recapitulates the *ufd-1* knockdown phenotypes

(A) Representative fluorescence images of N2 and ELT-2 overexpression (*elt-2*_OE) animals incubated on *P. aeruginosa*-GFP for 24 hours at 25°C after growth on *E. coli* OP50. Scale bar = 200 µm.

(B) Quantification of GFP levels of N2 and *elt-2*_OE animals incubated on *P. aeruginosa*-GFP for 24 hours at 25°C after growth on *E. coli* OP50. ***$P < 0.001$ via the *t*-test ($n = 30$ worms each).

(C) Representative survival plots of N2 and *elt-2*_OE animals on *P. aeruginosa* PA14 at 25°C after growth on *E. coli* OP50. The difference between the N2 and *elt-2*_OE survival plots is nonsignificant.

Table S1: Upregulated and downregulated genes in *ufd-1* RNAi versus empty vector (EV) control RNAi N2 animals. Genes exhibiting at least a two-fold change and *P*-value <0.01 were considered differentially expressed.